Synergy unleashed: *Leishmania donovani* GP63 paralogues cooperatively function to drive parasite infectivity at various pathogenic stages and regulate host survival mechanisms

Debolina Manna[1], Suvendu Nandi[1,*], Shounak Jana[1,*], Kristína Záhonová[2,3,4,5], Sunandini Bhattacharya[1], Deneshraj S[1], Nilanjan Pradhan[1], Nidhi Pandey[1], Debarati Biswas[1], Mahitosh Mandal[1], Gayatri Mukherjee[1], Vyacheslav Yurchenko[2], Budhaditya Mukherjee[1,#]

[1] School of Medical Science and Technology, Indian Institute of Technology Kharagpur, Kharagpur, India

[2] Life Science Research Centre, Faculty of Science, University of Ostrava, Ostrava, Czech Republic

[3] Institute of Parasitology, Biology Centre, Czech Academy of Sciences, České Budějovice, Czech Republic

[4] Department of Parasitology, Faculty of Science, Charles University, BIOCEV, Vestec, Czech Republic

[5] Division of Infectious Diseases, Department of Medicine, University of Alberta, Edmonton, Canada

* Equal contribution

[#] Corresponding author: aditya26884@gmail.com

ABSTRACT

Leishmania donovani (Ld), the etiological agent of visceral leishmaniasis, poses a significant global health burden due to its complex dixenous lifecycle involving both insect vectors and mammalian hosts. Successful infection in mammals requires the coordinated activity of stage-specific virulence factors. The zinc metalloprotease glycoprotease 63 (GP63) is a well-established virulence determinant critical for host cell attachment and invasion by insect-stage promastigotes. For humans, subsequent parasite propagation depends exclusively on intracellular amastigotes arising from lysed macrophages. Classical GP63 expression and function in Ld amastigotes remain poorly understood, and GP63 null mutants reportedly retain infectivity in mice, raising fundamental questions about virulence factor complementation during mammalian infection. By

employing comparative transcriptomics, CRISPR-based mutagenesis, complemented with cell biology, and biochemical assays, this work identifies and characterizes multiple Ld GP63 paralogues with distinct roles in mammalian infection. While both copies of GP63 encoded on chromosome 10 (LdGP63_10.51 and 10.52) were functionally redundant, LdGP63_28 encoded on chromosome 28 proved essential for intracellular amastigote survival by suppressing host cell pyroptosis. Moreover, LdGP63_31 (chromosome 31) was found to primarily mediate promastigote attachment to the host macrophages with minimal contribution from LdGP63_28, facilitating initial infection establishment and amastigote genesis. Importantly, the absence of LdGP63_28 impacted amastigote infection more severely as compared to LdGP63_31. Structural and enzymatic analyses revealed divergent localization and substrate specificities to fulfil functional requirement of these divergent proteases, which have evolved independently to carry out diverse function in establishing infection. Collectively, this study indicates evolutionary divergence and functional specialization among GP63 isoforms in Ld by demonstrating that amastigote-specific and promastigote-specific GP63 isoforms synergistically mediate infection establishment and persistence.

Keywords:

Leishmaniasis, virulence factors, metalloprotease, host-parasite interactions, pyroptosis

Introduction

Leishmaniases, a group of sandfly-transmitted diseases caused by *Leishmania* parasites, remain a pressing global health challenge, threatening over one billion people. The disease manifests along a spectrum from self-limiting cutaneous lesions to fatal visceral leishmaniasis (VL) caused by *Leishmania donovani* (Ld), which continues to cause about 30,000 cases annually. India accounts for nearly 18% of the global VL burden, highlighting its disproportionate impact on vulnerable populations.

Leishmania parasites follow a digenetic lifecycle, alternating between the flagellated promastigote stage in sandfly midgut and non-flagellated amastigote stage in mammalian host, requiring to adapt its infection machinery in two different phylogenetic host. To establish a successful infection in human, *Leishmania* parasites utilize a number of "virulent factors", which help them evade host cell mediated lysis, support attachment and entry into host and survive within host cells as infective amastigotes. These factors include lipophosphoglycan (LPG), phosphoglycan (PG), glycophosphatidylinositol and a zinc metalloprotease called leishmanolysin or glycoprotease 63 (GP63). Among all these factors, GP63, has been highlighted to be the most crucial virulence factor that plays a role in multiple host-signaling pathways affected by Leishmania infection, particularly in mammals with minimal role in sand fly host.

In humans, GP63 contributes to the early entry of promastigotes by allowing them to attach to and interact with host Complement receptor 1 (CR1) and complement receptor 3 (CR3), to block complement mediated lysis and promotes opsonization by aiding C3b conversion into iC3b. Thereby Ld promastigotes hijack lipid rafts on the host plasma membrane or upregulate vesicular fusion to gain access into the host. After the Ld promastigotes have successfully invaded the host macrophages (Mϕ) they transform into amastigotes within membrane bound parasitophorous vacuoles (PV) and continue to multiple intracellularly. However, the subsequent infectivity is mediated by these amastigotes which are released from apoptotic, lysed Mϕs into the host system. Unlike promastigotes, molecular cues which initiates and regulates this exit mechanism of intracellular amastigotes from infected visceral Mϕs and their subsequent entry in neighboring uninfected Mϕs remains a complete black box. Moreover, gp63 also represents one of the most heterogeneous gene families in the *Leishmania* genome, distributed across chromosomes 10, 28, and 31, with copy numbers varying from 4 in *L. donovani* and 7 in *L. major* to approximately 33 in *L. braziliensis*. This remarkable variation suggests lineage-specific adaptive divergence driven not only by the host species but also by the distinct host microenvironments in which the parasites persist. Extensive GP63 knockout studies in cutaneous *Leishmania* species such as *L. major* and *L. amazonensis* have shown that mice infected with classical chromosome 10 GP63-deficient mutants develop skin lesions more slowly than those infected with the wild type, but does not result in complete loss of infectivity. However, the role of GP63 in VL-causing strains remains completely unexplored.

These challenges coupled with the fact that some reports show a drastic drop in GP63 expression in amastigotes, thus raised a fundamental question- if amastigotes express minimal GP63, and classical GP63 is not indispensable to mice, as observed in *L. major* mutants, how do the amastigotes continue to persist within the host for prolonged infectivity? These questions were addressed in the present study, which aimed to identify and functionally characterize the Ld infectivity factor capable of complementing GP63 function in cutaneous infection, not only during the initial promastigote-driven infection but, more importantly, during the subsequent amastigote-

mediated phase. Initial *in silico* analysis using TriTrypDB and homology alignment with classical *L. major* GP63 (chromosome 10) revealed five putative proteases in Ld. CRISPR-based sequential Knock out of theses proteases revealed while two proteases (LdGP63_10.51 and LdGP63_10.52) situated on Ld chromosome 10, have lost their function and are dispensable for host infection, LdBPK_280600.1 on chromosome 28 and LdBPK_31 on chromosome 31 are non-dispensable for establishing successful host infection. Although, LdGP63_28_KO promastigotes, exhibited some degree of attachment and initial infection defect, most prominent effect of its absence was noticed on survival of intracellular amastigotes, as the KO amastigotes fail to prevent activation of host inflammatory pathways resulting in pyrophoric death of infected Mϕs. In contrast, LdGP63_31_KO promastigotes drastically failed to actively attach to the host Mϕs, and were taken up wrapped in dendritic protrusions extend from Mϕ membrane. This unusual entry consequently resulted in reduced amastigogenesis, which eventually gets cleared during early hours post host entry. This differential functional activity of LdGP63_28 and LdGP63_31 in host infection is also supported by their differential localization and substrate specificity. While LdGP63_28 is primarily localized in host cytoplasm cleaving cytoplasmic substrates like caspases, LdGP63_31 localized itself in the host plasma membrane lipid rafts, facilitating cleaving of C3b to iC3b fragments, required for entry of Ld promastigotes. Importantly, in terms of amastigote infection, LdGP63_28 showed a dominant potential over LdGP63_31, as the amastigote-specific protease, with both of its axenic and intracellular amastigotes failing to infect Mϕs. This study becomes imperative to define the roles of GP63, which might have evolved independently to execute specific functions in VL-causing strain, a work if properly ventured into can result in important vaccine targets for the fatal VL.

RESULTS

1. Identification of GP63 homologues in *L. donovani*

To identify amastigote-specific proteases potentially involved in *L. donovani* (Ld) virulence, an *in silico* screen was performed using TriTrypDB based on the presence of a protease domain, amastigote-specific expression in infected murine Mϕs (PMID- 26452044), and the presence of a signal peptide or transmembrane domain (**Fig. 1A.i**). This approach yielded five candidate genes, LdBPK_080950.1, LdBPK_080960.1, LdBPK_191460.1, LdBPK_100510.1, and LdBPK_280600.1 (**Fig. 1A.ii**). Among these, LdBPK_100510.1 and LdBPK_280600.1 corresponded to GP63, while LdBPK_080950.1, LdBPK_080960.1 and LdBPK_191460.1 encoded Cathepsin L-like and Cysteine peptidase A proteases. Multiple sequence alignment using the *L. major* GP63 sequence (Lm_GP63) crystal structure (obtained from PDB: 1LML) demonstrated conservation of the N-terminal, central, and C-terminal domains, along with catalytic motifs (PAVGVINIPA, HEXXH, KAREQYGC, and QDELMAP), exclusively in LdBPK_280600.1 (**Fig. 1B.i, ii**). However, LdBPK_100510.1 showed a truncated sequence lacking these key features. Comparative sequence alignment analyses showed that Lm_GP63 shared the greatest similarity with LdBPK_280600.1, supported by near-zero E-values, whereas the remaining candidates showed non-significant E-values (**Table 1**). Accordingly, LdBPK_280600.1 was prioritized as a probable amastigote-specific GP63 orthologue. AlphaFold structural superimposition of LdBPK_280600.1 with Lm_GP63 generated a TM score of 0.77998 and RMSD score of 1.763 which confirmed a perfect overlap of conserved residues (**Fig. 1B.iii–iv**, **Supp. Fig. 1**), reinforcing its sequence conservation. However, contrary to *in silico* predictions, qPCR analyses detected significant expression of both LdBPK_280600.1 and LdBPK_100510.1 in promastigote (**Fig. 1C.i**), axenic (**Fig. 1C.ii**), and intracellular amastigote stages (**Fig. 1C.iii**) across two independent clinical Ld isolates. Both were therefore included for downstream studies and designated as LdGP63_28 and LdGP63_10.51, respectively.

2. LdGP63_10.51 is highly expressed, but a non-functional protease

For functional characterization, endogenous C-terminal tagging of LdGP63_10.51 was carried out in Cas9-expressing Ld line (**Supp. Fig. 2A.i, ii**). Integration of the eGFP was confirmed by PCR in four independent clonal population three weeks post-transfection (**Supp. Fig. 2A.iii**). Localization studies showed diffuse cytosolic expression of LdGP63_10.51eGFP, with faint signal in the flagellum (**Supp. Fig. 2B.i**). Infection of primary murine Mϕs revealed LdGP63_10.51eGFP within host cytosol surrounding intracellular amastigotes, with significant translocation into the host nucleus at 24 h p.i. (**Supp Fig. 2B.ii**), consistent with qPCR profiles (**Fig. 1C**). Generation of LdGP63_10.51 knockout mutants (**Fig. 2A.i, ii**) produced no observable phenotypic defects. Independent KO clones displayed growth, morphology, and motility comparable to wild-type (WT) parental lines (**Fig. 2A.iii, iv**; **Video S1**), and showed no impairment in metacyclogenesis (**Fig. 2A.v.a,b**). Moreover, comparative attachment assays in primary murine Mϕs demonstrated that the KO lines attach to host Mϕs as efficiently as WT (**Fig. 2B.i, ii**; **Video S2**), which resulted in comparable number of intracellular amastigote numbers at 6 h, 24 h, and 48 h p.i. between KO and WT-infected Mϕs (**Fig. 2B.iii, iv**). This results thus confirm that the truncated LdGP63_10.51,

lacking a functional protease motif, is dispensable for both promastigote and amastigote stages of infection.

3. LdGP63_28 is essential for *L. donovani* amastigote persistence in infected Mϕ

Endogenous tagging (LdGP63_28mCherry) and knockout (LdGP63_28_KO) lines were generated in Cas9-expressing Ld as described for LdGP63_10.51 (**Fig. 3A, 3B**) and integration of the mCherry-puromycin cassette was PCR-confirmed (**Fig. 3A.i, ii**). Localization experiments revealed, unlike LdGP63_10.51, LdGP63_28 showed diffuse cytosolic distribution with minimal flagellar signal (**Fig. 3A.iii**). Expansion microscopy further pin down LdGP63_28 to have a punctuated vesicular appearance preferentially localized near flagellar pocket (**Fig. 3A.iv**), indicative of vesicular secretion. In infected Mϕs (**Fig. 3A.v**), LdGP63_28 signals were detected as vesicular structures within host cytosol, without any nuclear accumulation like LdGP63_10.51 (**Supp. Fig. 2B.ii**). Notably, LdGP63_28 vesicles were present not only in Ld infected Mϕ but also in neighbouring uninfected Mϕs, confirming its vesicular release (**Fig. 3A.v**). Interestingly, although, LdGP63_28_KO clones (**Fig. 3B.i, ii**) displayed no growth, morphology, or motility defects (**Fig. 3B.iii, iv**; **Video S3**), and normal metacyclogenesis (**Fig. 3B.v.a,b**), they showed a modest yet significantly reduced attachment to host with rounded and less motile promastigotes as compared to WT parental Ld (**Fig. 3C.i, ii**; **Video S4**). Surprisingly, more pronounced defect was observed in intracellular amastigotes proliferation with LdGP63_28_KO amastigotes number declining sharply by 24 h and almost becoming negligible by 48 h p.i. (**Fig. 3D.i, ii**). This disappearance of amastigotes was accompanied by decrease in number of host Mϕs (**Video S5**), with existing ones showing a granular, shrunken phenotype (**Supp. Fig. 3A.i, ii**), with elevated Annexin/PI positivity for LdGP63_28_KO infection (**Supp. Fig. 3B**). These observations indicate impaired macrophage persistence during infection with LdGP63_28_KO, likely resulting from heightened pro-inflammatory activation that may trigger pyroptotic cell death in host Mϕs. Complementation with WT-GFP LdGP63_28 restored host attachment (**Fig. 3C.i, ii**) and vesicular localization in host cytosol (**Fig. 3D.i**), rescuing amastigote persistence (**Fig. 3D.ii**), confirming LdGP63_28 as essential factor for promastigote adhesion and amastigote survival.

4. LdGP63_28_KO mutants cause nuclear fragmentation and cell death of infected host by inducing pyroptosis

Suspecting that LdGP63_28_KO infection, unlike the parental line, causes pyroptosis of infected Mϕs, this was further examined by staining of CD11b, a surface macrophage protein. At 6 h p.i., both infections showed intact membranes and nuclei, however, by 24-48 h p.i., LdGP63_28_KO infected Mϕs displayed progressive membrane fragmentation with occasional nuclear rupture (**Fig. 4A**). The punctate disintegration of macrophage membranes in KO infections, absent in parental infections suggests that LdGP63_28 loss promotes in infected host pyroptosis rather than apoptosis. Contrarily, flow cytometry at 24 h p.i. detected significant increase of Annexin V signal in only KO infections compared to uninfected and parental controls (**Fig. 4B**), indicating involvement of apoptosis along with pyroptosis. At 48 h p.i., low cell counts precluded flow cytometry analysis, but qPCR revealed marked upregulation of *nlrp3*, *caspase 3*, *caspase 2*, *caspase 7*, *caspase 1*, and to some extent in aim2, but not *nlrc4*, in KO infections (**Supp. Fig. 4**),

consistent with apoptotic and pyroptotic host death. Notably, *nlrp1* was upregulated in both infection types, but declined over time in parental infections while remaining high in KO infections. Western blot (**Fig. 4C**) confirmed NLRP3 upregulation at 24 h and 48 h in KO infections, along with activation/cleavage of Caspase 1, Caspase 3, and Gasdermin E, suggesting a preferential pyroptotic cascade activation, though apoptosis could not be excluded. Notably, sustained cleaved IL-1β was detected at 48 h in KO infections but diminished in parental infections also indicated persistent pyroptotic response through NLRP1 activation. Finally, SEM imaging (**Fig. 4D**) further showed membrane disintegration and "pyroptotic bodies" without nuclear fragmentation, confirming host Mϕs mostly suffer pyroptotic death in absence of LdGP63_28.

In vivo experiments in BALB/c mice showed almost comparable splenic parasite load in KO infections and parental at 12 days p.i, but by 24 days p.i., KO load decreased wrt parental load (**Fig. 4E.**).

5. *L. donovani* relies on distinct GP63 paralogues to assist in their host entry and intracellular survival

Since LdGP63_28 showed minimal involvement in host attachment and invasion, additional homologues were investigated for potential roles in host infection. The phylogenetic analysis of with the full-length LdGP63, identified GP63 proteins of selected *Leishmania* spp and *Angomonas deanei* used as an outgroup (**Fig. 5A., Supple Fig. 5**) identified three separate clades each containing sequences from different *Leishmania* spp. chromosomes. Phylogenetic tree thus identified LdBPK_312040.1 (henceforth LdGP63_31) and LdBPK_100520.1 (henceforth LdGP63_10.52), apart from LdGP63_28 and LdGP63_10.51, which were not identified in TryTripDB analysis (**Fig 1.A.i., ii.**). The phylogeny thus suggested independent evolution of the GP63 paralogues, implying their functional divergence. Multiple sequence alignment of all Ld GP63 paralogues revealed that, like LdGP63_10.51, LdGP63_10.52 lacked catalytic motifs, indicating a non-functional protease, while LdGP63_31 retained conserved active-site residues similar to LdGP63_28 (**Supp. Fig. 6A**). Functional analysis confirmed that LdGP63_10.52_KO parasites (**Supp. Fig. 6B.i, ii**) displayed no change in morphology, growth, or macrophage infection (**Supp. Fig. 6B.iii–v, C.i, ii, D.i, ii**), confirming its non-essential nature.Knockout of LdGP63_31 (**Supp. Fig. 7A.i, ii**), also did not alter parasite morphology, growth, or motility (**Supp. Fig. 7A.iii–iv**; **Video S6**) and yielded metacyclic numbers comparable to the parental strain (**Supp. Fig. 7A.v.a, b**). Interestingly, two distinct parasite populations appeared within the metacyclic zone of LdGP63_31_KO (**Supp. Fig. 7A.v.a**), a feature absent in the parental and other knockout lines. Infection with LdGP63_31_KO resulted in a severe defect in host attachment (**Fig. 5B.i, ii**). Surprisingly, despite this, infection assays detected intracellular LdGP63_31_KO amastigotes at 6 h p.i., but their numbers dropped sharply by 24 h and were nearly absent by 48 h (**Fig. 5C**). However, in contrast to LdGP63_28_KO infections, Mϕs harbouring LdGP63_31_KO parasites appeared morphologically intact, showing pronounced dendritic extensions (as seen in bottom left image of **Fig 5C**) rather than apoptotic or pyroptotic features (**Video S7**; **Fig 5. D.**). Time-course analyses (**Fig. 5E.i**) revealed that the LdGP63_31_KO line established intracellular presence significantly earlier than the parental strain, within 30 min p.i. achieving a higher initial intracellular load that declined over time, producing a bell-shaped infection profile (**Fig. 5E.ii**).

Notably, despite this early establishment, LdGP63_31_KO promastigotes consistently exhibited reduced host attachment across all time points (**Fig. 5F**), consistent with earlier attachment assay (**Fig. 5B**). Importantly, the internalized LdGP63_31_KO parasites retained a spindle-shaped morphology with visible cytosol and flagella, indicative of defective amastigogenesis (**Fig. 6A**). Scanning electron microscopy further confirmed that, unlike the tight adhesive interactions of the parental parasites, LdGP63_31_KO promastigotes show a lateral attachment enveloped by macrophage dendritic projections (**Fig. 6B.i, ii**), suggesting that impaired attachment favours enhanced phagocytic uptake rather than direct invasion, leading to premature yet defective internalization. TEM imaging (**Fig 6C**).…Furthermore, GPI-anchor prediction also identified a putative GPI signal (**Fig. 6.D**), resembling Lm_GP63 and suggesting a potential role in host membrane attachment. Collectively, these findings indicate that LdGP63_31 plays a critical role in host membrane attachment required for proper entry and parasitophorous vacuole generation, essential for successful amastigogenesis and infection persistence.

6. LdGP63_28 and LdGP63_31 have differential host localization and substrate specificity

To explore the apparent distinct roles of LdGP63_28 and LdGP63_31 in host entry and amastigote persistence, their localization and substrate specificity were analyzed. LdGP63_31 was endogenously tagged with mNeonGreen in the LdGP63_28_mCherry line (**Supp. Fig. 7B.i, ii**) and used to infect murine Mϕs. In double-tagged promastigotes, LdGP63_28 displayed punctate cytosolic expression (**Fig. 7A.i**), as observed previously (**Fig. 3A.iv**), while LdGP63_31 was distributed across the cytosol, flagella, and cytoskeleton, partly co-localizing with β-tubulin (**Fig. 7A.i**). In infected Mϕs, LdGP63_28_mCherry was found to be localized to the cytosol, whereas LdGP63_31_mNeonGreen was enriched at the host membrane (**Fig. 7A.ii**). Colocalization with cholera toxin confirmed LdGP63_31 association with lipid rafts (**Fig. 7B.i**), and only LdGP63_31_KO parasites failed to recognize raft-rich regions (**Fig. 7B.ii**), affirming its role in host entry.

As data suggested, the dependence of the parasite on LdGP63_31 for attachment and on LdGP63_28 for intracellular survival, their substrate preferences were assessed. Docking and 100 ns molecular dynamics simulations with known Lm_GP63 substrates with distinct host localizations (**Supp. Fig. 8A, 8B**) showed similar binding capacities for both the proteases. Thus, to further investigate differential substrate specificity, recombinant LdGP63_28 (**Fig. 8A.i, iii**) and LdGP63_31 (**Fig. 8A.ii, iv**) were purified (**Fig. 8A.v**) and confirmed to be catalytically active by zymography (**Fig. 8A.vi**). *In vitro* enzymatic cleavage assays confirmed functional divergence, with LdGP63_28 cleaving cytosolic mTOR, while LdGP63_31 specifically processing membrane-bound C3b to yield cleaved C3b and iC3b fragments (**Fig. 8B**). Notably, LdGP63_28 produced only cleaved C3b and not iC3b, again confirming its minimal role in Ld entry apart from maintenance of intracellular amastigotes. Neither protease degraded c-Jun or β-actin. Collectively, LdGP63_31 mediates host attachment *via* lipid-raft interactions, whereas LdGP63_28 mostly facilitates intracellular survival by targeting cytosolic substrates.

7. LdGP63_28 plays a critical role in re-invasion and egress in amastigote stage of Ld

To investigate which of these proteases are important for amastigote infection, axenic amastigotes from double-tagged LdGP63_28mCherry–LdGP63_31mNeonGreen lines were purified, and expression of both proteases was confirmed in axenic and intracellular amastigotes by confocal microscopy (**Fig. 9A.i**). Subsequent infections with both these double-tagged amastigotes also showed that, as with Ld promastigote infection, in amastigote infection also, LdGP63_28 maintained punctate cytosolic localization in hosts, while LdGP63_31 remained membrane-associated (**Fig. 9A.ii**), suggesting both may participate in amastigote infection, contrary to RNA-seq predictions. Next, axenic amastigotes generated from parental, LdGP63_28_KO and LdGP63_31_KO Ld lines were used to infect Mϕs (**Fig. 9B**). Interestingly, although LdGP63_31_KO parasites exhibited reduced amastigogenesis (**Video S8**), which was confirmed by SEM imaging (**Fig 9C**). SEM analysis confirmed these morphological differences with LdGP63_31_KO amastigotes appearing thicker, longer, and often tailed, while LdGP63_28_KO forms were mildly elongated but largely flagella-deficient (**Fig. 9C.i, ii**), However, despite these compromised amastigogenesis, LdGP63_31_KO axenic amastigotes still retained significant infection capacity, whereas LdGP63_28_KO axenic amastigotes completely failed to establish infection at 24 h p.i, supporting a stronger role for LdGP63_28 in amastigote invasion. (**Fig. 9D.i, ii**). However, re-infection assays with syringe-lysed intracellular amastigotes from parental, LdGP63_28_KO, and LdGP63_31_KO lines into fresh Mϕs revealed, unlike axenic infections, both KO forms showed marked loss of re-infection ability (**Fig. 9E.i-iii**). Therefore, while both proteases may contribute, LdGP63_28 plays a more prominent role in amastigote re-infection. This difference in infectivity between axenic and intracellular amastigotes of LdGP63_31_KO, might also result from loss of viability of isolated intracellular amastigotes as LdGP63_31_KO amastigotes fails to sustain in within host macrophages, and get cleared within a very short period of time, compromising their fitness to re-infect.

DISCUSSION

Visceral leishmaniasis (VL) remains a major public health concern, with rising drug unresponsiveness and the absence of a vaccine complicating treatment and causing approximately 30,000 deaths annually. These challenges have emphasized the need for alternative therapeutic targets that can act against both extracellular promastigotes and intracellular amastigotes to block human transmission. GP63, a zinc metalloprotease, has long been recognized as a pivotal virulence factor in *Leishmania* spp, particularly in cutaneous forms like *L. major*. However, its specific roles and druggability in human visceral infection caused by *L. donovani* (Ld) have remained largely unexplored. In this study, distinct functional roles of individual GP63 paralogues were characterized, providing a refined understanding of their differential contributions to Ld infectivity.

Two GP63 paralogues, located on chromosomes 10 (LdGP63_10.1) and 28 (LdGP63_28), were initially identified based on sequence similarity with *L. major* classical GP63. Unlike *L. major*, where the chromosome 10 paralogue functions as the major protease, GP63_10.1 in Ld was found to be truncated, lacking the catalytic domain and enzymatically inactive. Despite being expressed in both promastigotes and infected macrophages, knockout of GP63_10.1 caused no detectable phenotypic changes, suggesting evolutionary divergence in GP63 functionality between cutaneous and visceral species. Conversely, LdGP63_28 retained an intact active site and displayed vesicular cytosolic localization both in promastigotes, in infected and adjacent uninfected macrophages, implicating its role in early interactions between host and Ld. While LdGP63_28_KO promastigotes showed no major growth defect, their infectivity and host cell attachment were moderately compromised. Strikingly, LdGP63_28_KO amastigotes failed to persist in macrophages and were unable to suppress host inflammatory responses, leading to parasite clearance. These results indicate that LdGP63_28 modulates host cell death pathways, promoting amastigote survival within macrophages. Importantly, these results also identified pyroptotic cell death rather than apoptosis as a major form of cell death in LdGP63_28 KO infected Mϕs, with prominent cell membrane rupture and formation of pyroptotic bodies, with intact nucleus. Pyroptosis involves upregulation of inflammasomal proteins like AIM1, NLRP3 or NLRC1, followed by cleaving of inflammatory caspases, like caspase-1, and release of inflammatory cytokines, such as IL-1b and IL-18 through the pore-forming Gasdermins, while in apoptosis there is no involvement of inflammation and continues via initiator caspases (caspase 2, caspase 8, etc) and executioner caspases (caspase 6, caspase 7, etc), Activation of Caspase-3 along with cleaving of Gasdermin-E, a pathway well defined for pyroptotic cell death, also confirmed a specific skewing towards pyroptosis rather than apoptosis in absence of LdGP63_28. It is important to note that pyroptosis has also been widely observed during pathogen invasion, including infection of *Leishmania* spp.

Phylogenetic analyses revealed two additional GP63 paralogues, LdGP63_31 (chromosome 31) and LdGP63_10.52 (chromosome 10). Knockout of LdGP63_31 resulted in a pronounced defect in macrophage attachment and an unusually rapid yet aberrant internalization, mediated by lateral interactions with dendritic protrusions. This defective entry disrupted amastigote differentiation and led to early parasite clearance without inducing apoptosis, suggesting that LdGP63_28 and LdGP63_31 operate independently at distinct stages of infection. Localization studies confirmed that LdGP63_31 is GPI-anchored and enriched in lipid rafts during parasite entry, consistent with its proposed role in membrane-cytoskeleton remodeling.

Differential substrate processing further emphasized the functional divergence of the two proteases. LdGP63_28 preferentially cleaved cytosolic substrates, including inflammasome components, whereas LdGP63_31 targeted membrane-associated complement proteins like C3b, converting them into inactive iC3b to facilitate immune evasion.
In the amastigote stage, transformation efficiency of knockout parasites revealed further functional segregation. LdGP63_28_KO promastigotes successfully differentiated into axenic amastigotes, while LdGP63_31_KO parasites largely retained promastigote morphology. However, despite this, infection assays demonstrated a sharper loss of infectivity for LdGP63_28_KO amastigotes compared to LdGP63_31_KO, underscoring the essentiality of LdGP63_28 in amastigote infection. Reinfection experiments with intracellular amastigotes yielded similar outcomes, confirming near-complete loss of infectivity for both knockouts. However, this difference in infectivity between axenic and intracellular amastigotes of LdGP63_31_KO, might also result from loss of viability of isolated intracellular amastigotes as LdGP63_31_KO amastigotes fails to sustain in within host macrophages, and get cleared within a very short period of time, compromising their fitness to re-infect.Together, these findings highlight the functional evolution of GP63 paralogues in *L. donovani*, with LdGP63_28 maintaining intracellular niche stability and LdGP63_31 orchestrating host attachment and entry mechanisms critical for establishing infection.

MATERIALS AND METHODS

Animals

BALB/c mice were maintained and bred under pathogen-free conditions with food supplements and filtered water. All experiments were conducted in accordance to Institutional Animal Ethics Committee (IAEC), IIT Kharagpur guidelines India (IAEC/BI/1 55/2021) and approved by National Regulatory Guidelines issued by Committee for the Purpose of Supervision of Experiments on Animals, Ministry of Environment and Forest, Government of India.

In-silico analysis for protease identification

In silico analysis to identify the probable amastigote-stage proteases was performed in TriTrypDB Release 58 (https://tritrypdb.org/tritrypdb/app) and is shown schematically in **Fig. 1.A.i**. First, under the “Search Strategies” tool, we selected “Text (product name, notes, etc.) from the “Gene Searches”. Next, in this “Identify Genes based on Text” section, *L. mexicana* (reference strain MHOM/GT/2001/U1103) was selected and “*protease” was mentioned as the “wildcard” in “text term”. Then, the “Add a step” option was chosen to select “Transcriptomics” followed by “RNA-Seq Evidence” where the data-set “Promastigote, Axenic Amastigote and Intracellular Amastigote Transcriptomes”; “DE” was further selected for analysis. “PRO” was selected as “reference sample”, while “AMA” was the “comparator sample”. All other parameters were left as default. The resultant genes from the RNAseq dataset were “intersected with” the *L. mexicana* and this yielded 44 genes. By using the “edit” feature on these 44 genes, orthologs of these differentially expressed genes in *L. donovani* (reference strain BPK282A1) were found (36 genes), and a nested strategy to eliminate genes containing no transmembrane and no signal peptide domain was built by the “Add a step” feature, where “Predicted Signal Peptide” and “Transmembrane Domain Count” of *L. donovani* (reference strain BPK282A1) were “united” with Boolean operation,

thus generating 8 genes. Finally, the "Orthologs" feature was added from the "Edit" option, eventually producing 5 hits.

Sequence alignment and annotation

The sequences of the five identified *L. donovani* (LD) protease genes LdBPK_080950.1, LdBPK_080960.1, LdBPK_191460.1, LdBPK_100510.1 and LdBPK_280600.1 were retrieved from TriTrypDB and aligned with the already available *L. major* GP63 (LmjF.10.0460, Lm_GP63) crystal structure sequence (PDB: 1LML) using the MUSCLE MSA tool by EMBL-EBI (https://www.ebi.ac.uk/jdispatcher/msa/muscle).

The alignment file was further annotated in ESPript 3.0 beginner mode. PDB: 1LML was uploaded as the secondary structure, and labels were set to α1, β1, α2, β2. Considering the crystal structure of Lm_GP63 as the reference, the N-terminal, Central and C-terminal domains were labelled highlighting the conserved regions (PAVGVINIPA, KAREQYGC and QDELMAP) and HEXXH active site. Schematic diagrams highlighting the domains and sites was generated using DOG 2.0 - Protein Domain Structure Visualization.

Pairwise Sequence Alignment of LD orthologues with GP63 was performed both locally and globally, using EMBOSS Water (Waterman-Smith) and EMBOSS Needle (Needleman-Wunsch Algorithm) respectively. The Expect-value (E-value) was calculated from NCBI-BLAST.

Homology modelling

All the 3D structures were visualized using PyMOL v2.5, and missing residues were modelled using ALPHAFOLD. TM-Scores were provided by TM-Align tool by Zhang Lab (https://aideepmed.com/TM-align/), while the RMSD scores of LdGP63_28 and LdGP63_31 aligned with Lm_GP63 were provided by PyMOL v2.5 using the "Align" plugin.

RT-PCR Analysis

For gene expression analysis, 2 x 10^8 log-phase promastigotes and axenic amastigotes, or murine Mϕs infected with Ld amastigotes were harvested and RNA extraction process was performed according to the RNeasy Mini kit protocol (Qiagen). To synthesize complementary DNA (cDNA), 2 μg of RNA was reverse-transcribed using the ProtoScript® II First Strand cDNA Synthesis Kit (NEB). Quantitative RT-PCR was then performed with 200 ng of cDNA per sample using SYBR Green Master Mix (Applied Biosystems). Data were analyzed by 2-ΔΔCt methods through normalization with GAPDH or beta-actin. The thermal cycling conditions were 94°C for 10 minutes, followed by 40 cycles at 94°C for 15 seconds and 60°C for 1 minute. Primers used for all RT-PCR reactions have been mentioned in Table 2.

Maintenance of parasite strains

Promastigotes of Ld strain MHOM/IN/09/BHU575/0 and all other mutant strains were cultured at 22°C in M199 medium (Sigma-Aldrich) supplemented with 5% Nusera (Himedia). The appropriate selection drugs (SRL) were added to the medium at the following concentrations: 200 µg/ml hygromycin B, 200µg/ml blasticidin dihydrochloride, 200µg/ml G418 and 200 µg/ml puromycin dihydrochloride.

Generation of endogenously tagged and knockout parasite strains

To generate Ld cell lines that stably express Cas9 and T7 polymerase pTB007 (Beneke, Madden et al., 2017) plasmid was transfected into Ld promastigotes and Cas9 expression was confirmed by western blotting, as mentioned later. All the primers for tagging and knockout were retrieved from the LeishGEdit website [42, 43].
pPLOTv1 puro-mCherry-puro (Beneke, Madden et al., 2017), pPLOTv1 blast-mNeonGreen-blast (Beneke, Madden et al., 2017) and pPLOTv1 puro-eGFP-puro (cloned in the lab) were used to endogenously tag the C-terminals of LdGP63_28, LdGP63_31 and LdGP63_10.52, respectively. Briefly, the 3′ sgRNA template was amplified using the Downstream_sgRNA and G00 primer, whereas mCherry-puro, mNeonGreen-blast and eGFP-puro cassettes were amplified from their respective plasmids using Q5 High-Fidelity DNA Polymerase (New England Biolabs). The drug-resistant cassettes and sgRNA were pooled followed by transfection into Ld-Cas9,
To generate knockouts, the 3′ sgRNA and 5' sgRNA templates was amplified using the Downstream_sgRNA and G00 and Upstream_sgRNA and G00 primers, respectively. Puromycin and blasticidin resistance cassettes were amplified from pTpuro v1 and pTblast v1 plasmids, respectively, with Q5 High-Fidelity DNA Polymerase (New England Biolabs) and were together transfected into Ld-Cas9.

Parasite transfections

For all transfections, 1 x 10^{10} parasites were mixed in a 2mm cuvette with the relevant plasmid (20ug) or amplified DNA (approx. 60 µl) in about 340ul of 1x electroporation buffer (21mM HEPES, 137mM NaCl, 5mM KCl, 0.7mM NaH2PO4, 6mM glucose), and electroporated using a BTX Electroporation system with 2 pulses at 450V, 500µF and 25ohm. Electroporated cells were immediately kept on ice for 5minutes and then transferred into M199 medium (substituted with 10% FCS) and left to recover overnight before adding selection drugs. Drug-resistant mutants were confirmed about 10 days after transfection reactions.

DNA Extraction and Confirmative PCRs

For PCR verification of genetically modified parasite strains and for cloning genes into plasmids, DNA was extracted using the DNAsure mini kit (Qiagen) and PCRs were performed using GoTaq DNA Polymerase (Promega).
Primers used for the PCR have been mentioned in Table 2.

Promastigote Growth Curve analysis

Approximately 1 x 10^5 wild type and KO promastigotes were cultured in 10% FBS supplemented M199 media and counted in a Neubauer chamber daily for up to 7 days. Data points were plotted on Graph Pad Prism to generate the graph.

Scanning electron microscopy

The promastigotes or Mϕs adhered in the polylysine-coated coverslips were further processed for SEM. Briefly, the promastigotes or Mϕs were washed with PBS followed by incubation for 1hour in 5% Osmium tetroxide with careful addition or removal of osmium tetroxide under a fume hood. Then, increasing ethanol gradient dehydration using 70%, 80%, 90%, and finally 100% was performed twice each step covering 10 mins. After final incubation, ethanol was removed and completely airdried. Dry coverslips were stored in a vacuum desiccator till imaging. On the

imaging day, sections were sputtered by gold using Quorum Q150R ES and proceeded for imaging using Field Emission- Merlin, Zeiss Sigma 300 VP and JEOL scanning electron microscopy unit.

Flow cytometry of metacyclic Ld

The Ld promastigotes were washed and resuspended in PBS before being subjected to light scatter analysis using flow cytometry. Ld population were checked with forward scatter (FSC) versus side scatter (SSC) and dot plot was generated to represent the acquisition of 10,000 events using a FACS Aria II system. Histogram to compare between parental and knockout strains, each with three replicates, was plotted in Graph Pad Prism.

Cell Culture and Infection

Peritoneal Mϕs were harvested from BALB/c mice as mentioned in already published protocol, with slight modifications. After 48h of mice intraperitoneal injection with 4% starch, Mϕs were isolated and plated on 35-mm petri dishes or on sterile coverslips in 24-well plates at a density of $2x10^6$ or $1.5x10^5$, respectively, and allowed to grow in RPMI 1640 medium (Gibco) supplemented with 10% (v/v) Nusera (Himedia) and 1% (v/v) Penicillin-Streptomycin solution (Gibco). The cells were allowed to adhere for 48h at 37°C in 5% CO_2. Then, Mϕs were infected with stationary-phase promastigotes at a 1:10 ratio (10 parasites per Mϕ) for 6h. The Mϕs were then washed with 1x PBS to remove any extracellular loosely attached parasites and incubated further as per experimental requirements.

Promastigote attachment assay

The attachment of promastigotes to the murine Mϕs was studied by the protocol mentioned in (). Briefly, $1.5x10^5$ parasites were added to Mϕs already seeded on a 24 well plate, by resuspending in RPMI 1640 medium, followed centrifuging at 720g at 4C for 5min. The plate was then incubated at 4C for 5minutes and cells were fixed with ice cold methanol. This was followed by Giemsa staining and the coverslips, affixed onto glass slides, were examined under Olympus light microscope. Attached parasites were counted and plotted with respect to 100 Mϕs.

Intracellular parasite infection

To study intracellular amastigote infectivity, resting stage Mϕs on glass coverslips were infected with metacyclic-stage sorted parental or mutant strains of Ld promastigotes at a ratio of 1:10, as described previously. Following a 6h incubation, the Mϕs were washed with 1x PBS and subsequently cultured for specific time points as per experimental requirements. Coverslips were retrieved at necessary time points, rinsed with 1x PBS, fixed using ice-cold methanol or 2% paraformaldehyde, as necessary, and either stained with Giemsa or proceeded for immunofluorescence staining. These prepared coverslips were then affixed onto glass slides and examined utilizing a either light microscope (Olympus) or confocal microscope, as mentioned later. Parasite quantification was conducted by counting number of amastigotes per 100 Mϕs.

Immunofluorescence assay and confocal microscopy

To prepare promastigotes for confocal microscope imaging, cultured stationary phase parasites at a number of $1*10^4$ were pelleted down in a 1.5ml centrifuge tube followed by resuspending it in 1x PBS. Then a drop of parasites was layered onto a coverslip and fixed in 2%

paraformaldehyde for 3 min. Coverslips were then kept in neutralization buffer (0.1M glycine in PBS). For Mϕ-infected amastigotes, as mentioned in the infection protocol previously, coverslips at the experimental time points were collected, rinsed with 1x PBS, fixed with 2% paraformaldehyde for 3 min and kept in neutralization buffer. The PFA fixed parasites or Mϕs were then permeabilized using 0.2% Triton/PBS for 20 min on an orbital shaker. For cell membrane staining, this permeabilization step was omitted. Non-specific binding was blocked with 2% BSA in 0.2% Triton/PBS for another 20 min on an orbital shaker. The parasites or Mϕs were then incubated with primary antibodies for 1 hr, followed by washing and staining with IgG Alexa Fluor 594 or IgG Alexa Fluor 488, as required. Mounting was performed using Fluromount-G-DAPI (Thermo Scientific) and observed under Olympus confocal microscope (FV3000) or Leica Stellaris microscope using appropriate fluorescence emission filters, and photographed. 3D image visualization was processed through Fiji 3D viewer and 3D project plugin.

Annexin-PI cell death assay

Parental or KO strains were allowed to infect Mϕs and incubated for 48h p.i. with an intermediate PBS wash at 6h p.i. Initially, the cells were scraped, pelleted down by centrifuging at 1200rpm, washed with PBS followed by resuspending in FACS buffer. However, this protocol resulted in maximum cell death (>80% cell death) in untreated and parental treated Mϕs as well, possibly due to mechanical stress of scraping. To minimize cell death, a number of buffer systems were experimented with and eventually 10mM EDTA in 1x PBS (detach solution) was used to detach the cells. Infected cells submerged in detach solution were incubated at 4C for 15 minutes, and then the detach solution was vigorously pipetted to dislodge the cells. Detached cells were harvested by centrifuging at 1200rpm at 4C. Annexin-V and PI stains were added to the cells and incubated on ice for 15 minutes. The presence or absence of Annexin V-FITC or PI was then checked by FACS Aria II system as per experimental requirements.

GPI-anchor prediction

NetGPI 1.1 (https://services.healthtech.dtu.dk/services/NetGPI-1.1/) tool was used to predict the presence GPI-anchors in the protease.

In vivo infection

For in vivo infections, healthy female BALB/c mice (4–6 weeks old and 20–25 g each) were injected via tail vein route with 1×10^7 Parental-dsred2 or LdGP63_28_KO-dsred2 expressing *L. donovani* stationary phase metacyclic promastigotes (suspended in 100 µl 1× phosphate-buffered saline [PBS]) as reported previously (Khanra et al., 2020). Each group contained two mice that were sacrificed 12 days and 24 days post-infection (p.i). Splenocytes were isolated and dsred2-positive population was measured through flow cytometry. Each experiment was performed in triplicate.

Generation of addback strains

To generate addback strains, LdGP63_28 was cloned into pXG-eGFP plasmid and the pXG-eGFP-LdGP63_28 clone was then transfected into LdGP63_28_KO promastigotes, with the same protocol as mentioned previously. LdGP63_31 was cloned into pXG-eGFP by Twist Biosciences. Similar to LdGP63_28_addback, pXG-eGFP-LdGP63_31 clone was also

transfected into LdGP63_31_KO. Post-transfections, parasites were allowed to recover for 10 days and episomal expression of LdGP63_28 and LdGP63_31 was confirmed by PCR.

Cloning LdGP63_28 and LdGP63_31 into pGEX-6p-1

From the genomic DNA of Ld promastigotes, previously isolated with DNASure Tissue Mini Kit (Nucleopore), LdGP63_28 (1629bp) and LdGP6_31 (1911bp) were amplified using the primers mentioned in Table 2. Amplified LdGP63_28 and LdGP63_31 and linear pGEX-6p-1 were run on agarose gels by electrophoresis and target bands were visualized under UV-transilluminator and excised from the gels followed by gel purification (Gel and PCR purification Kit, Promega). Cloning of LdGP63_28 or LdGP63_31 into pGEX-6p-1, containing GST tag, was carried out by incubating them with NEBuilder mastermix at 50C for 1 hour. The ligated product was transformed into competent *E. coli* (DH5α) cells followed by plating on Ampicillin-LB agar plate, which was incubated overnight at 37°C. Colonies from transformed plate was picked and plasmid was isolated with Surespin Plasmid Miniprep Kit (Nucleopore) to screen for the positive by performing PCR with Go Taq polymerase.

Recombinant LdGP63_28 and LdGP63_31 production

Positive plasmid clones were transformed into *E. coli* Rossetta (DE3) by heat shock method and spread on to ampicillin-LB agar plates. Colonies from the plate were picked and cultured in LB medium with ampicillin selection, overnight. For secondary culture, 1% from the overnight primary culture was added to it, and allowed to grow at 37°C at 220rpm continuous shaking. When optical density (OD600) values at 600nm reached 0.6, 1mM IPTG was added to the secondary culture and kept for 5 hours with all other parameters intact. The bacteria were then harvested at 3200 g at 4°C, for 15 minutes, and the recombinant proteins were purified using the previously described protocol. In brief, cell pellet was lysed in PBS containing 1% Triton X-100 and protease inhibitor cocktail followed by freeze-thawing in liquid nitrogen and sonication. After lysis, protein supernatant was collected by spinning sonicated samples at 13000g. LdGP63_28-GST and LdGP63_31-GST was isolated by using Glutathione-Sepharose beads, followed by purification by adding reduced glutathione. The purified proteins were separately passed through endotoxin removal column (Pierce, Thermoscientific, USA) and then subjected to Size Exclusion Chromatography (SEC) for further purification. The SEC purified fractions were finally concentrated using Amicon® Ultra-15 Centrifugal Filter Unit (Milipore). The purified proteins were then visualized and confirmed by SDS-PAGE and western blotting, and used for further enzymatic assays.

SDS-PAGE and Western Blot

Samples were prepared by heating in 2x Laemmli buffer for 10 min at 95°C. The samples were subjected to SDS-PAGE (Bio-Rad) system on 8% SDS-polyacrylamide gels. Visualization of proteins on SDS-polyacrylamide gel was done by overnight staining with Coomassie Brilliant Blue R-250 solution.For western blotting, SDS-polyacrylamide gel was transferred to nitrocellulose membrane (GE Healthcare) in the presence of 1x transfer buffer (Tris-58.2g, Glycine-29.3g, 20% methanol) at 20 V for 50 minutes. The membrane was kept in blocking buffer [5% Skim milk powder (SRL) and PBST (1x PBS and 0.05%v/v Tween 20)] at 4°C for 1 hour, then probed in rabbit anti-GST antibody (Abclonal), overnight, then washed with PBST, incubated in goat anti-

rabbit peroxidase (Cell Signaling) antibody for 2 hours followed by washing with PBST. Bands were visualized with Chemiluminescent substrate (Cytiva).

Zymography assay

Gelatin zymography of the purified recombinant proteases was performed as per previously described protocol. Briefly, samples were mixed with loading dye without beta-mercaptoethanol and were loaded without boiling on a 10% SDS-PAGE gel containing 1.2 mg/ml of gelatin. Following SDS-PAGE, gels were incubated for 1 h in a buffer containing 50 mM Tris pH 7.4, 2.5% TritonX100, 5 mM $CaCl_2$ and 1 μM ZnCl for 1 h at RT. Gels were then briefly rinsed in distilled water and incubated overnight in a buffer containing 50 mM Tris pH 7.4, 5 mM $CaCl_2$ and 1 μM ZnCl at 37°C. Gels were then stained and briefly destained using Coomassie blue and visualized in Chemidoc.

Protein-Protein docking of substrates with homology-modeled protease

Ld_GP63_28 and Lm_GP63 were blind-docked individually with some known substrates of GP63, using the HADDOCK web server. Binding affinity was determined for each interaction with the PRODIGY web server, and further PyMOL was used to visualize the docked structures. LIGPLOT+ program was used for identifying the residues of the enzymes that interact with the substrates and these residues were further annotated in PyMOL.

Enzyme-substrate assay

Mϕs were washed 3X with cold PBS containing 1 mM of Na_3VO_4, scraped off using cell scraper and lysed on ice by repeated pipetting in 100 μL of 50 mM Tris-HCl (pH 7.5), 150 mM NaCl, 1 mM EDTA (pH 8), 1.5 mM EGTA, 1 mM Na_3VO_4, 50 mM NaF, 10 mM $Na_4P_2O_7$, and a mixture of protease and phosphatase inhibitors. It was followed by collecting the cells in a microcentrifuge tube, subjecting the tube to sonication for 10s burst and 10s gap for 2mins, centrifuging the tube at 3000rpm and collecting the supernatant or the cell lysate. Protein quantification was done with a nanodrop according to the protocol provided by the manufacturer. After protein quantification, the recombinant proteases were separately added to two different tubes containing rLdGP63_28 and rLdGP63_31 and incubated at 37°C for 1 hour. Then the tubes were boiled at 95°C for 10 min in Laemmli buffer and migrated in SDS-PAGE gels followed by Western Blotting as per the protocol mentioned above.

Amastigote generation and harvesting

Axenic amastigotes were generated by following a previously published protocol, with slight modifications. $1x10^4$ Promastigotes were harvested and resuspended in M199 media (pH=5.5) supplemented with 5% FBS. The parasites were allowed to incubate in 22C with constant shaking for 2 days, and then incubated in 37C for 2 more days. The parasite culture was then centrifuged at 2000rpm and the resultant pellet containing larger promastigotes were discarded. The supernatant was again centrifuged at 6000rpm to yield pellet of axenic amastigotes, which were then used for SEM imaging or infecting Mϕs, as required.

For intracellular macrophage isolation, Mϕs plated on 35mm cell culture petriplate were allowed to be infected with promastigotes for about 24h with an intermediate PBS wash at 6h to remove unbound parasites. At 24h p.i. the infected Mϕs were washed with PBS and detached from the petriplate using cell scraper, followed by repeatedly passing for about 6 times through the needle

of a 1ml syringe. The cells were then centrifuged at 1000rpm for 5 minutes to remove cell debris, and the supernatant collected was centrifuged at 6000rpm. The amastigote pellet thus collected was then used for Mϕ infection experiments.

Statistical analysis

All statistical analyses were performed using GraphPad Prism 8 on raw datasets to ensure robust and reproducible results. For datasets involving comparisons across multiple conditions, one- or two-way ANOVA was conducted, followed by Tukey's post hoc test to assess pairwise differences while controlling for multiple comparisons. A 95% CI was applied to determine the statistical reliability of the observed differences. For non-parametric comparisons across multiple groups, Wilcoxon rank-sum tests were employed, maintaining a 95% CI, which is particularly useful for analysing skewed data distributions. In cases where only two groups were compared, Student's *t*-test was used to determine statistical significance, ensuring an accurate assessment of mean differences. All quantitative data are represented as mean ± SEM to illustrate variability within experimental replicates. Statistical significance was determined at $p \leq 0.05$. Notation for significance levels: $^{*}p \leq 0.05$; $^{**}p \leq 0.001$; $^{***}p \leq 0.0001$.

LIST OF FIGURES AND FIGURE LEGENDS

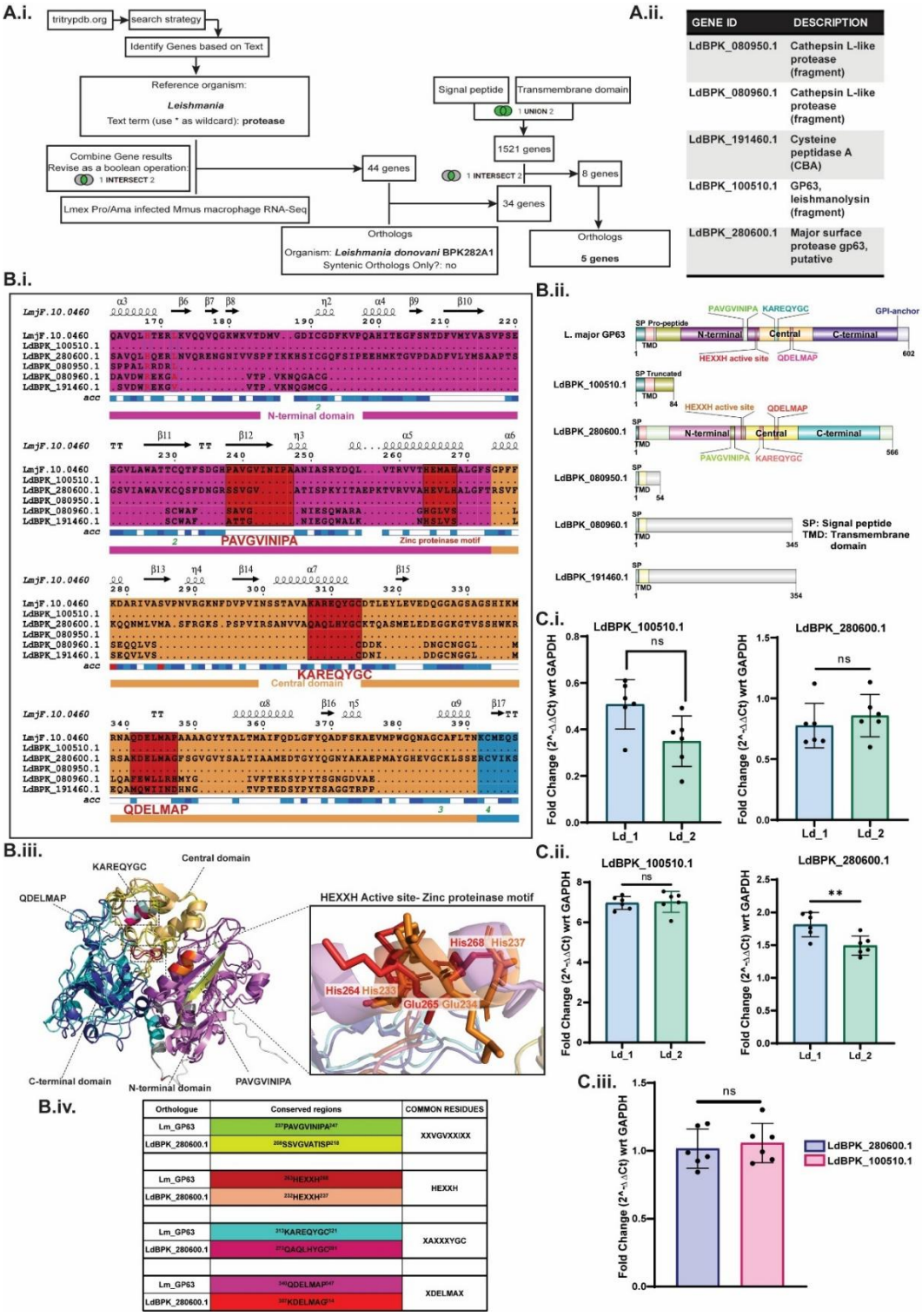

Figure 1: LdBPK_100510.1 and LdBPK_280600.1 might function as probable amastigote-specific proteases.

A. (i) Schematic representation of the strategy undertaken to sort potential amastigote proteases in TriTrypDB. A. (ii) List of the ‘5 hits’ obtained from the aforementioned strategy.

B. (i) Multiple sequence alignment of the 5 hits with *L. major* GP63 (Lm_GP63) showing the active site HEXXH, PAVGVINIPA, KAREQYGC and QDELMAP conserved regions marked in red. B. (ii) Simplified illustration of the presence or absence of conserved regions and active site in the identified hits with respect to Lm_GP63. B. (iii) Crystal structure of Lm_GP63 (PDB: 1LML) superimposed onto the Alphafold modelled LdBPK_280600.1 showing overlaps of the HEXXH active site (also zoomed to show the amino acid residues) and conserved regions within the N-terminal (Lm_GP63: magenta, LdBPK_280600.1: pink), Central (Lm_GP63: ochre, LdBPK_280600.1: light yellow) and C-terminal (Lm_GP63: dark blue, LdBPK_280600.1: cyan). B. (iv) Table comparing the amino acid residues between Lm_GP63 and LdBPK_280600.1; same colour codes corresponding to the conserved regions have been provided to B. ii, B. iii and B. iv.

C. qPCR analysis showing expression of LdBPK_100510.1 and LdBPK_280600.1 in two independent Ld strains in (i) promastigotes, P=0.0743 and P=0.3674 (ii) axenic amastigotes, P=0.8234 and P=0.0019 (iii) Ld infected murine Mϕs 6h p.i., P=0.6301. (n = 6 each data point represents one biologically independent replicate; ns P>0.05. *P < 0.05. **P < 0.01. Data represent the mean ± SEM. Differences between two groups were analyzed by unpaired two-tailed Student's t tests. Differences among more than two groups were analyzed by one way ANOVA.)

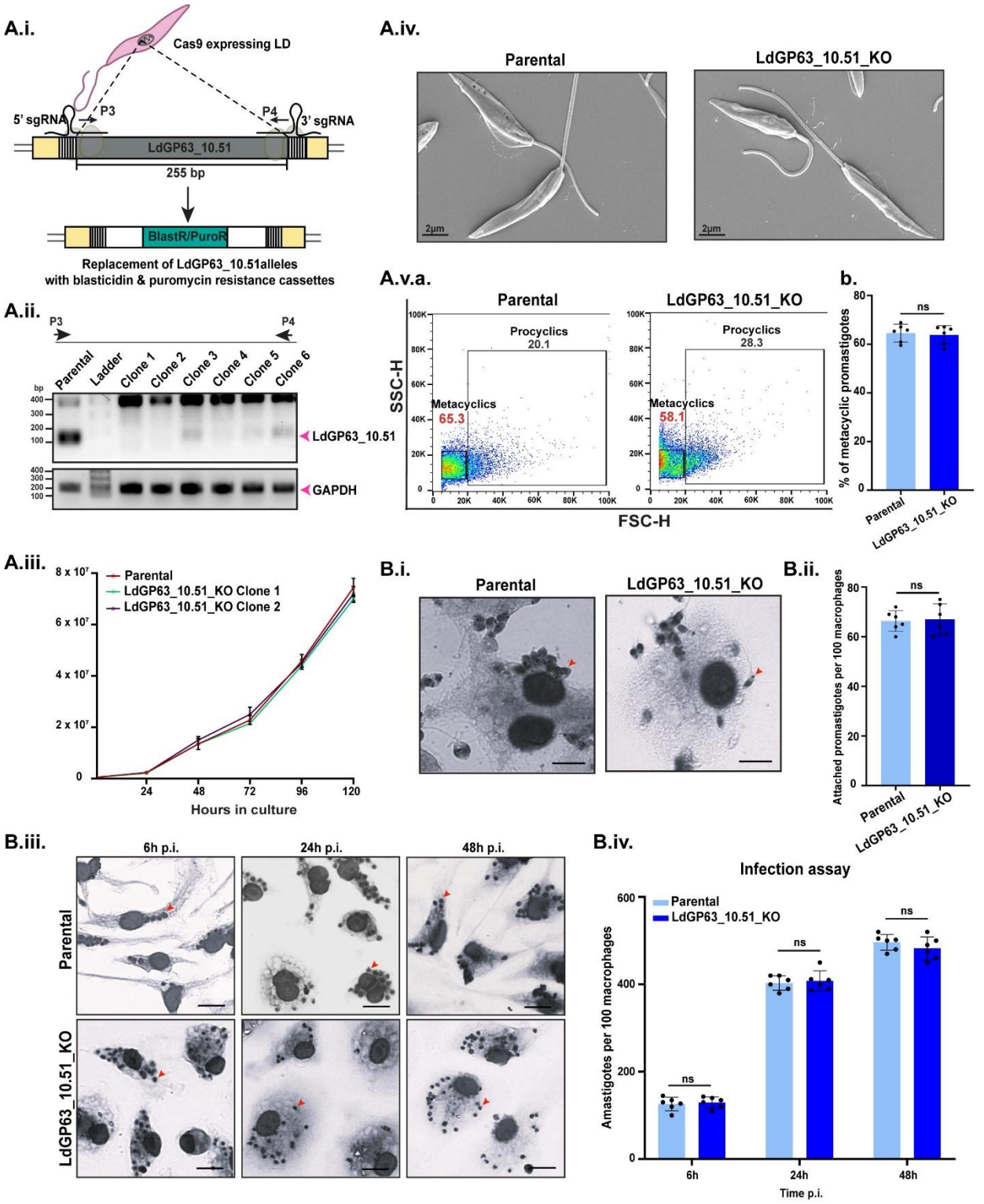

Figure 2: LdGP63_10.51 is not an essential protease for Ld infectivity.

A. (i) Schematic representation for knock out generation of LdGP63_10.51. A. (ii) Confirmatory PCR to identify LdGP63_10.51_KO from independent clonal populations represented as Clone 1.-6. GAPDH is the housekeeping control A. (iii) Growth curve to compare the replicative potential of selected clones (clone 1 and clone 2) w.r.t. parental. A. (iv) Representative SEM images of parental and KO promastigotes. Scale

bar is 2μm. A. (v) Flow cytometry plot to quantify number of metacyclics in stationary stage promastigotes of parental and which KO (a) with graphical representation (b) (P=0.7749). B. i. Giemsa-stained images comparing initial attachment at 30min p.i. ii. Representative bar graph showing number of attached parental and KO promastigotes (P=0.7935). B. iii. Giemsa-stained images of murine Mϕs infected with parental vs KO lines at 6h, 24h and 48h p.i. (iv) Representative graph showing the infection and proliferation of parental and KO amastigotes(P=0.8792). (n = 6 each data represents one biologically independent replicate; ns P>0.05. *P < 0.05. **P < 0.01. Data represent the mean ± SEM. Differences between two groups were analyzed by unpaired two-tailed Student's t tests. Differences among more than two groups were analyzed by one way ANOVA.)

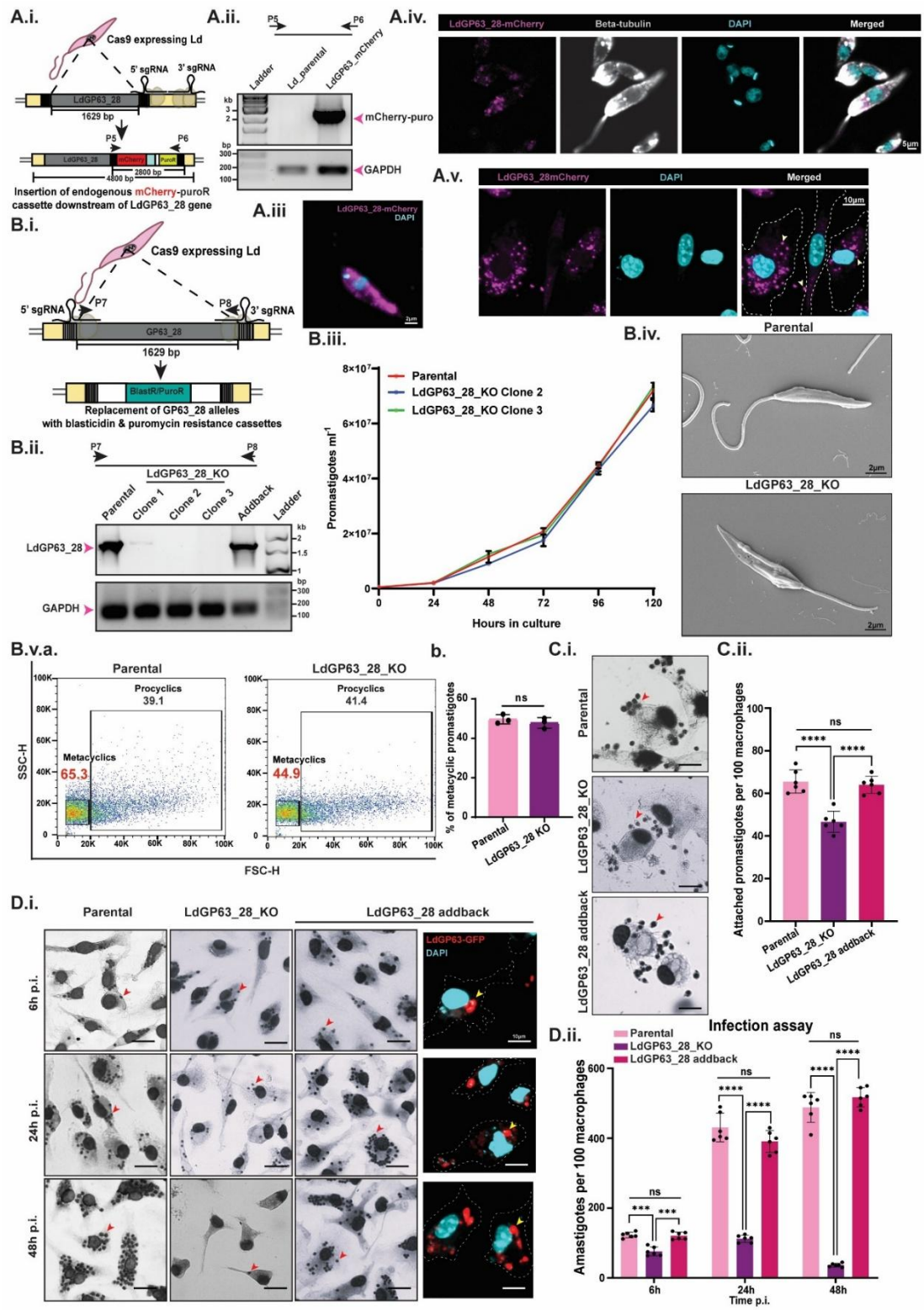

Figure 3: LdGP63_28 plays an essential role in infectivity and intracellular proliferation of Ld amastigotes.

A. (i) Scheme depicting the endogenous tagging of mCherry-puro cassette to the C-terminal end of LdGP63_28. A. (ii) PCR confirmation of inserted mCherry cassette downstream of LdGP63_28. GAPDH is

the housekeeping control. A. (iii). Confocal micrograph showing localization of LdGP63_28mCherry (labelled in magenta) in promastigotes. A. (iv) Confocal micrograph of promastigotes with ultraexpansion to visualize LdGP6_28mCherry w.r.t. beta-tubulin in promastigotes. A. (v) Confocal micrograph showing localization of LdGP63_28mCherry in infected amastigotes at 6h p.i. Scale bar is 2μm for iii., 5μm for iv. and 10μm for v.

B. (i) Schematic representation to knock out LdGP63_28. B. (ii) Confirmatory PCR to identify LdGP63_28_KO from independent clonal populations. B. (iii) Growth curve to compare the replicative potential of selected clones (clone 2 and clone 3) w.r.t. parental. B. (iv) Representative SEM images of parental and KO promastigotes. Scale bar is 2μm. B. (v) Flow cytometry plot to represent number of metacyclics in stationary stage promastigotes of parental and KO (a) with graphical representation (b) (P=0.7749).

C. i. Giemsa-stained images comparing initial attachment at 30min p.i. C. ii. Representative graph showing number of attached promastigotes between parental and KO.

D. i. Giemsa-stained images of murine Mϕs infected with parental and KO amastigotes at 6h, 24h and 48h p.i. D. (ii) Representative graph showing the infection and proliferation of parental and KO amastigotes. ($n = 6$ each data represents one biologically independent replicate; ns $P>0.05$. *$P < 0.05$. **$P < 0.01$. ***$P<0.005$. ****$P<0.0001$. Data represent the mean ± SEM. Differences between two groups were analyzed by unpaired two-tailed Student's t tests. Differences among more than two groups were analyzed by one way ANOVA.)

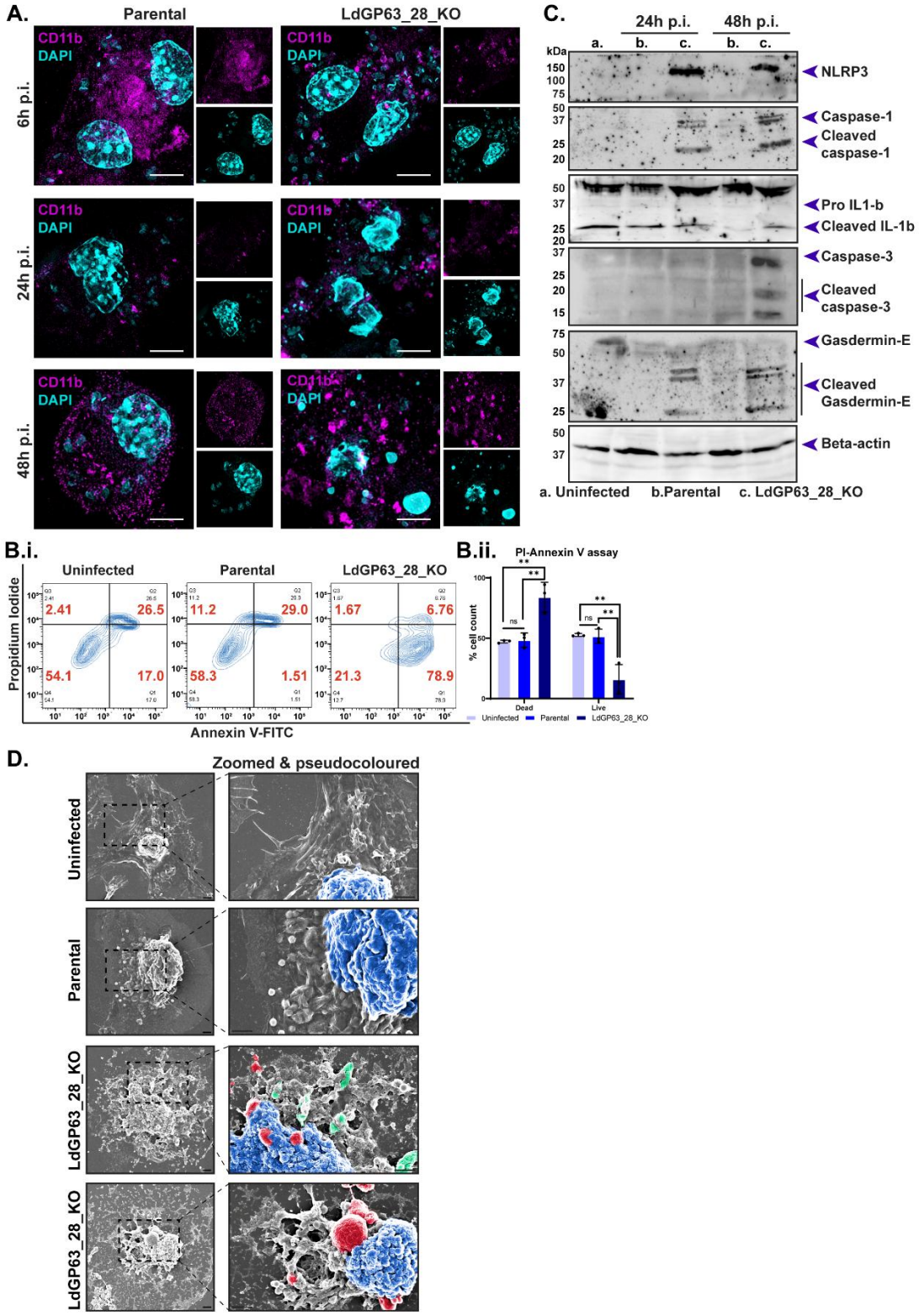

Figure 4: LdGP63_28 regulates pyroptosis by dampening inflammasomal responses.

A. Confocal micrographs showing the presence of CD11b in parental and LdGP63_28_KO infected Mϕs at 6h, 24h and 48h p.i.

B.i. Contour plot showing PI-Annexin V stained cells comparing uninfected, parental and LdGP63_28_KO 48h p.i. Mϕs, followed by graphical quantification data (B.ii.)
C. Western blot to quantify pyroptotic markers- NLRP3, caspase 1, IL-1b, caspase 3 and Gasdermin-E in parental vs KO infected Mϕs. Beta-actin is used as the housekeeping control.
D. SEM images of uninfected, parental and KO infected Mϕs showing nuclear region (blue), pyroptotic bodies (red) and dead parasites (green).
E. Flow cytometric plot to show dsRed2 count in splenocytes of uninfected, parental and KO infected Balb/C mice at 12days and 24days p.i.

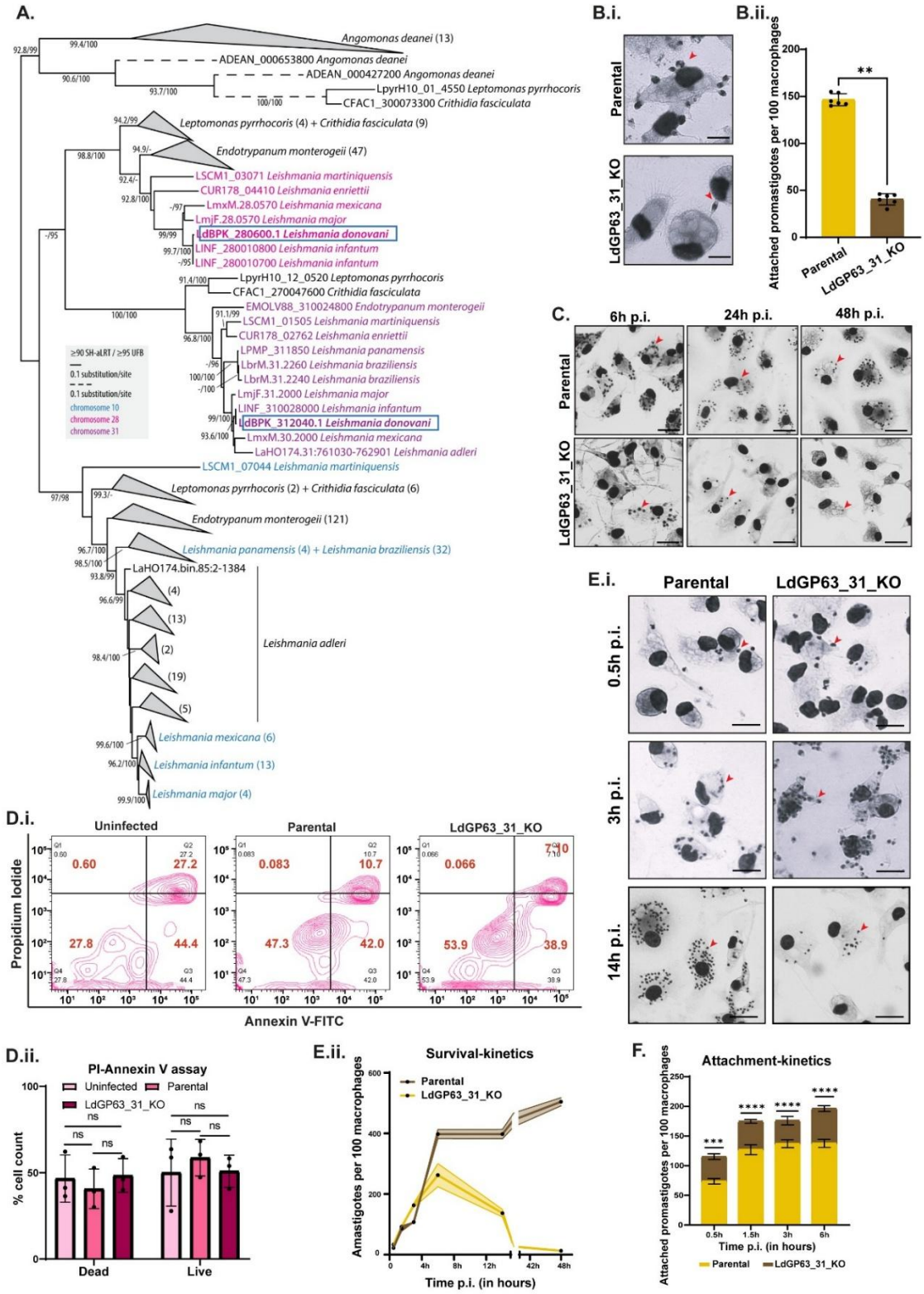

Figure 5: Loss of LdGP63_31 impairs the attachment and initial entry of Ld promastigotes, leading to defective entry of Ld.

A. Phylogenetic tree of Trypanosomatida GP63, with a special focus on *L. donovani*. The tree represents a subset of the complete phylogenetic timetree in Supplementary Fig. 5.
B. i. Giemsa-stained images comparing initial attachment at 30min p.i. ii. Representative graph showing number of attached parental and KO promastigotes. Scale bar is 5µm.
C. i. Giemsa-stained images of murine Mϕs infected with parental vs KO lines at 6h, 24h and 48h p.i.
D.i. Contour plot showing PI-Annexin V stained cells comparing uninfected, parental and LdGP63_31_KO 48h p.i. Mϕs, followed by graphical quantification data (D.ii.)
E. Giemsa-stained images of parental and KO infected Mϕs at 0.5h, 3h and 14h p.i. (i), followed by an amastigote survival graph comparing the number of amastigotes from 30min up to 48h p.i. in parental vs KO infected Mϕs (ii). E. (ii) Graph showing the attachment kinetics of parental and KO. Scale bar is 10µm. (n = 6 each data represents one biologically independent replicate; ns P>0.05. *P < 0.05. **P < 0.01. ***P<0.005. ****P<0.0001. Data represent the mean ± SEM. Differences between two groups were analyzed by unpaired two-tailed Student's t tests. Differences among more than two groups were analyzed by one way ANOVA).

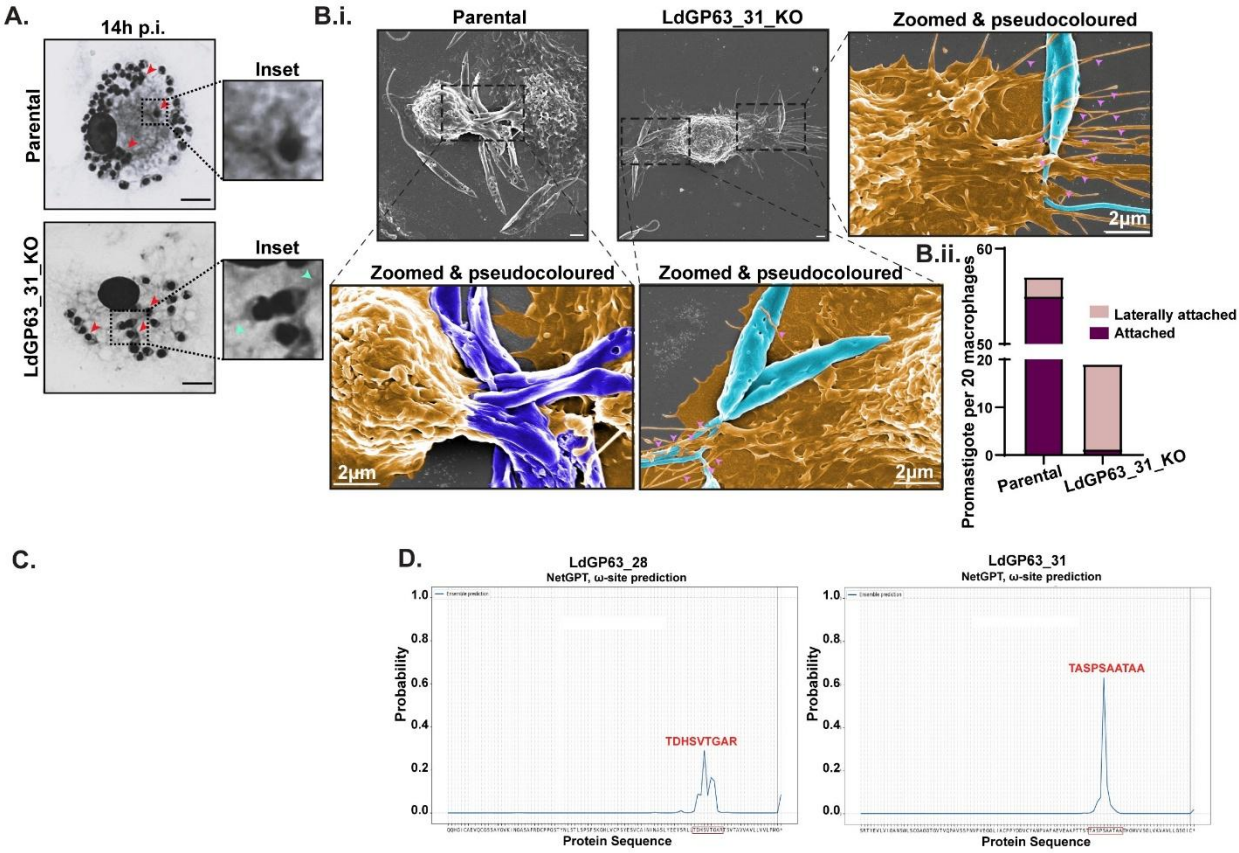

Figure 6: LdGP63_31_KO disrupts amastigogenesis with lateral attachment phenotype in promastigotes
A. Magnified image of infected Mϕs of parental vs KO at 14h p.i., with intracellular amastigotes highlighted in red arrows and parasite tail highlighted in green arrows. Scale bar is 10µm.
B. i. Representative SEM images depicting the attachment of parental (purple) vs LdGP63_31_KO (cyan) promastigotes to Mϕs. Dendritic projections are marked in pink arrows. ii. Graph highlighting the number of actively attached and laterally attached KO promastigotes w.r.t. parental.
C. TEM image

D. NetGPI plots to predict the presence of GPI- site in LdGP63_28 and LdGP63_31.

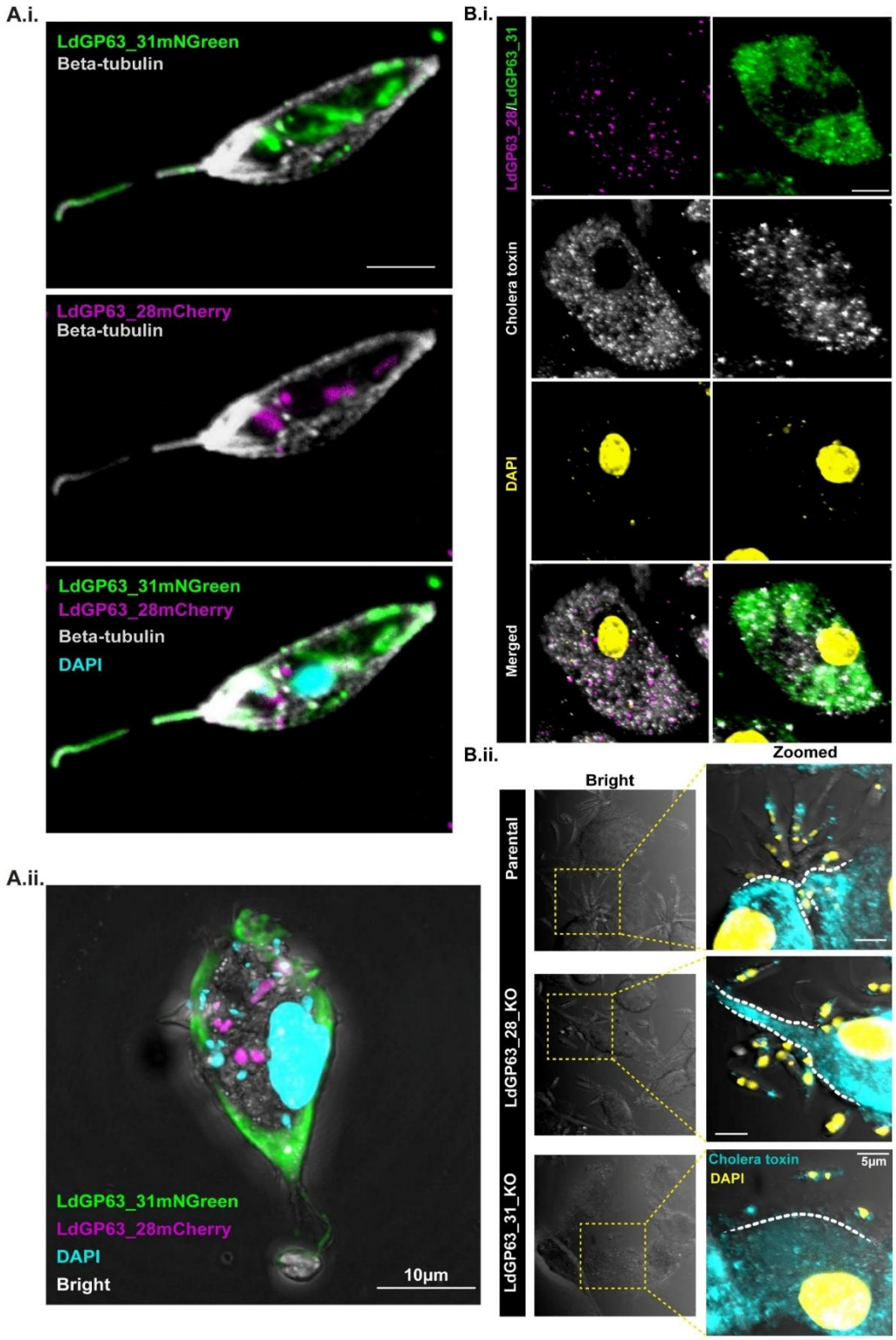

Figure 7: LdGP63_31 localizes in host membrane during Ld entry.

A. i. Confocal micrographs showing LdGP6_31mNGreen (Green) and LdGP63_28mCherry (Magenta) expression w.r.t. beta-tubulin in ultraexpanded promastigotes. Scale bar is 5 µm. A. ii. Confocal micrographs showing the localization of LdGP63_31mNGreen (Green) and LdGP63_28mCherry (Magenta) in 6h infected Mϕs. Scale bar is 10 µm.
B. i. Confocal micrographs to compare the cytoskeletal localization of LdGP63_31mNGreen (green) and LdGP63_28mCherry (magenta) with lipid raft marker Cholera toxin (grey). Scale bar is 10 µm. B. ii. DIC images showing attached LdGP63_28__KO and LdGP63_31_KO parasites to Mϕs (left panel), followed by confocal micrographs highlighting the interaction of attached parasites with cholera toxin, labelled in cyan (right panel). White dotted line demarcates the cell membrane, a point of contact between promastigotes and lipid raft. Scale bar is 2 µm.

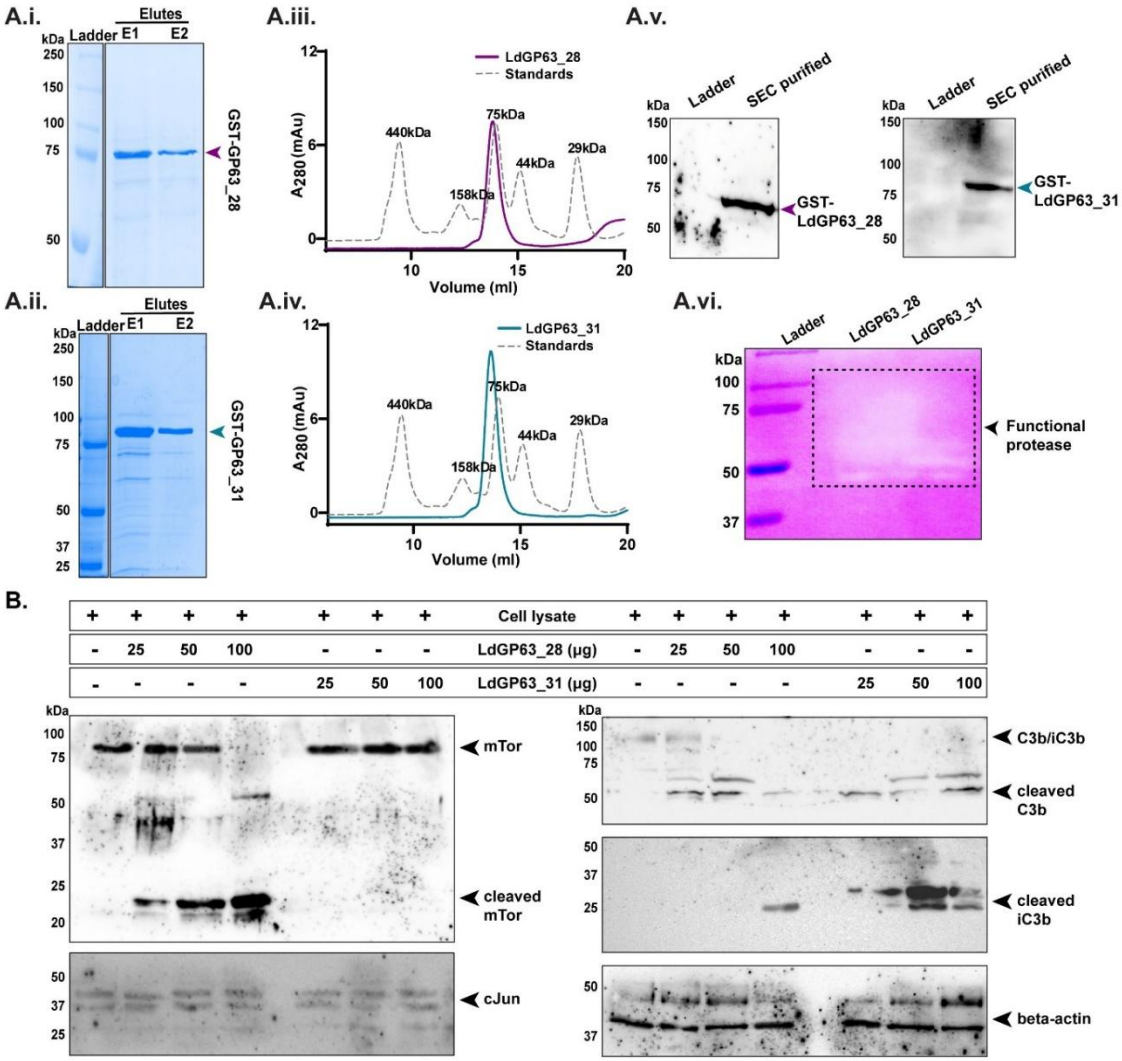

Figure 8: LdGP63_28 and LdGP63_31 have differential substrate specificities.
A. Coomassie blue stained gel showing glutathione affinity purified fractions of LdGP63_28(i) nd LdGP63_31 (ii), followed by their size exclusion chromatrogram (SEC) peaks (A. iii, iv) and western blots of the SEC purified fractions (A. v). A. vi. Zymogram of the SEC purified active proteases visualized on SDS-PAGE gel.

B. Western blots analysis of mTor, C3b and cJun of Mϕ lysate in absence and presence of recombinant LdGP63_28 and LdGP63_31 in varying concentrations of 25 µg, 50 µg and 100 µg. Beta-actin is used as the loading control.

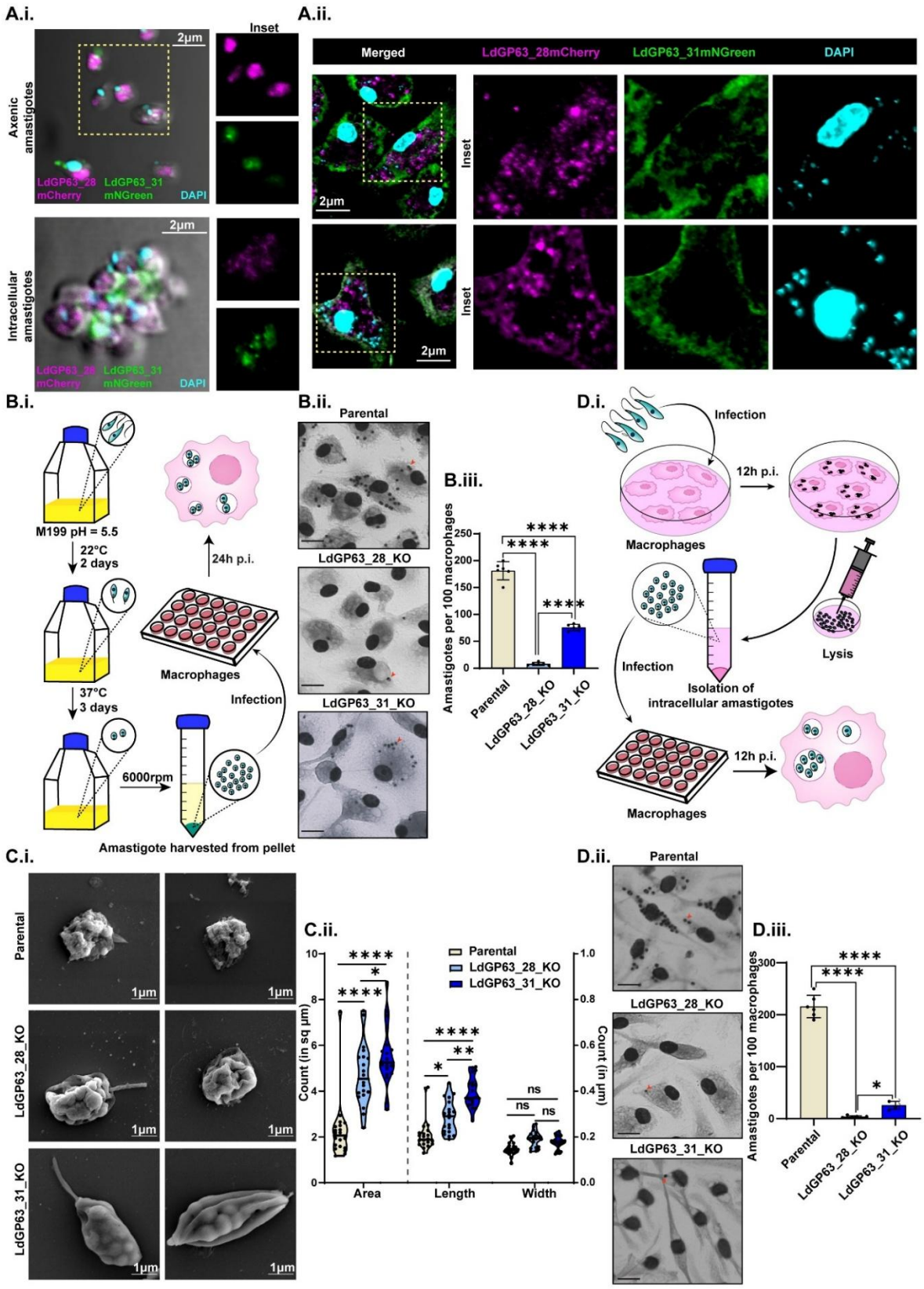

Figure 9: LdGP63_28 plays a critical role in amastigote infection.

A. i. Axenic and intracellular amastigotes of GP63_28mCherry-Gp63_31mNGreen showing expression of LdGP63_28 (Magenta) and LdGP63_31 (Green). Scale bar is 2µm. A. ii. Localization of LdGP63_28 (magenta) and LdGP63_31 (green) in axenic (top panel) and intracellular (bottom panel) amastigotes infected Mϕs. Scale bar is 2µm.
B. i. Scheme illustrating the generation of axenic amastigotes for further Mϕ infection assay, followed by (ii) Giemsa-stained images of LdGP63_28_KO and LdGP63_31_KO axenic amastigote infected Mϕ. Scale bar is 10µm.
C. i. SEM micrographs comparing axenic amastigotes of parental, LdGP63_28_KO and LdGP63_31_KO with stumped flagella (left panel) and no flagella (right panel), with representative graph (ii). Scale bar is 1µm.
D. i. Scheme illustrating the isolation of intracellular amastigotes from infected Mϕs and reinfection of fresh Mϕs. ii. Giemsa-stained images of Mϕs infected with intracellular amastigotes, followed by representative graph (iii). Scale bar is 10µm.

LIST OF TABLES

Table 1: Alignment scores of sorted virulent genes with *L. major* GP63

	Orthologue vs Lm_GP63						
	Global Alignment (Needleman-Wunsch)			Local Alignment (Smith-Waterman)			
Orthologues	Identity	Similarity	Gaps	Identity	Similarity	Gaps	E-value
LdBPK_080950.1	3.7	5	91	29.4	44.1	8.8	NS
LdBPK_080960.1	11.5	19.6	53.9	21.9	36.4	24.1	NS
LdBPK_191460.1	7.1	12.3	75.1	19.9	31.2	33	NS
LdBPK_100510.1	6	6.1	93.2	90	92	0	4e-113
LdBPK_280600.1	34.6	50.7	16.3	37.1	54	11.2	5e-10

NS: Non-Significant

ACKNOWLEDGEMENT

Funding was provided to DM by CSIR. Authors would like to acknowledge IIR lab, SMST, IITKGP for their help with flow cytometric analysis, confocal microscope facility of Department of Biotechnology, DST-FIST, Govt. of India, and confocal facility of SMST. Authors would like to thank all the interns of the IDI lab, SMST who help in various experiments related to this project. Computational resources were provided by the e-INFRA CZ project (ID:90254), supported by the Ministry of Education, Youth and Sports of the Czech Republic.

REFERENCES

Arango Duque, G. and A. Descoteaux (2015). "Leishmania survival in the macrophage: where the ends justify the means." Current Opinion in Microbiology 26: 32-40.

Bahr, V., et al. (1993). "Expression of lipophosphoglycan, high-molecular weight phosphoglycan and glycoprotein 63 in promastigotes and amastigotes of Leishmania mexicana." Molecular and Biochemical Parasitology 58(1): 107-121.

Beneke, T. and E. Gluenz (2019). LeishGEdit: A Method for Rapid Gene Knockout and Tagging Using CRISPR-Cas9. Leishmania: Methods and Protocols. J. Clos. New York, NY, Springer New York: 189-210.

Beneke, T., et al. (2017). "A CRISPR Cas9 high-throughput genome editing toolkit for kinetoplastids." Royal Society Open Science 4(5): 170095.

Bhattacharya, S., et al. (2024). "Deciphering the intricate dynamics of inflammasome regulation in visceral and post-kala-azar dermal leishmaniasis: A meta-analysis of consistencies." Acta Tropica 257: 107313.

Castro Neto, A. L., et al. (2019). "In silico characterization of multiple genes encoding the GP63 virulence protein from Leishmania braziliensis: identification of sources of variation and putative roles in immune evasion." BMC Genomics 20(1): 118.

Chan, A., et al. (2022). "The role of Leishmania GP63 in the modulation of innate inflammatory response to Leishmania major infection." PLOS ONE 16(12): e0262158.

Colovos, C. and T. O. Yeates (1993). "Verification of protein structures: Patterns of nonbonded atomic interactions." Protein Science 2(9): 1511-1519.

Contreras, I., et al. (2010). "Leishmania-Induced Inactivation of the Macrophage Transcription Factor AP-1 Is Mediated by the Parasite Metalloprotease GP63." PLOS Pathogens 6(10): e1001148.

Cuervo, P., et al. (2008). "Cellular localization and expression of gp63 homologous metalloproteases in Leishmania (Viannia) braziliensis strains." Acta Tropica 106(3): 143-148.

de Sá, K. S. G., et al. (2023). "Gasdermin-D activation promotes NLRP3 activation and host resistance to Leishmania infection." Nature Communications 14(1): 1049.

Debrabant, A., et al. (2004). "Generation of Leishmania donovani axenic amastigotes: their growth and biological characteristics." International Journal for Parasitology 34(2): 205-217.

Edgar, R. C. (2004). "MUSCLE: multiple sequence alignment with high accuracy and high throughput." Nucleic Acids Research 32(5): 1792-1797.

Fiebig, M., et al. (2015). "Comparative Life Cycle Transcriptomics Revises Leishmania mexicana Genome Annotation and Links a Chromosome Duplication with Parasitism of Vertebrates." PLOS Pathogens 11(10): e1005186.

Frommel, T. O., et al. (1990). "The major surface glycoprotein (GP63) is present in both life stages of Leishmania." Molecular and Biochemical Parasitology 38(1): 25-32.

Gíslason, M. H., et al. (2021). "Prediction of GPI-anchored proteins with pointer neural networks." Current Research in Biotechnology 3: 6-13.

Gomez, M. A., et al. (2009). "Leishmania GP63 Alters Host Signaling Through Cleavage-Activated Protein Tyrosine Phosphatases." Science Signaling 2(90): ra58-ra58.

Goris, M., et al. (2024). "NLRP1-dependent activation of Gasdermin D in neutrophils controls cutaneous leishmaniasis." PLOS Pathogens 20(9): e1012527.

Guay-Vincent, M.-M., et al. (2022). "Revisiting Leishmania GP63 host cell targets reveals a limited spectrum of substrates." PLOS Pathogens 18(10): e1010640.

Hallgren, J., et al. (2022). "DeepTMHMM predicts alpha and beta transmembrane proteins using deep neural networks." bioRxiv: 2022.2004.2008.487609.

Harper, S. and D. W. Speicher (2011). "Purification of proteins fused to glutathione S-transferase." Methods Mol Biol 681: 259-280.

Hassani, K., et al. (2014). "Absence of Metalloprotease GP63 Alters the Protein Content of Leishmania Exosomes." PLOS ONE 9(4): e95007.

Hsiao, C.-H. C., et al. (2008). "The major surface protease (MSP or GP63) in the intracellular amastigote stage of Leishmania chagasi." Molecular and Biochemical Parasitology 157(2): 148-159.

Ilg, T., et al. (1993). "The lysosomal gp63-related protein in Leishmania mexicana amastigotes is a soluble metalloproteinase with an acidic pH optimum." FEBS Letters 327(1): 103-107.

Isnard, A., et al. (2012). "Impact of Leishmania metalloprotease GP63 on macrophage signaling." Frontiers in Cellular and Infection Microbiology Volume 2 - 2012.

Jaramillo, M., et al. (2011). "Leishmania Repression of Host Translation through mTOR Cleavage Is Required for Parasite Survival and Infection." Cell Host & Microbe 9(4): 331-341.

Jumper, J., et al. (2021). "Highly accurate protein structure prediction with AlphaFold." Nature 596(7873): 583-589.

Kamran, M., et al. (2023). "The paradigm of intracellular parasite survival and drug resistance in leishmanial parasite through genome plasticity and epigenetics: Perception and future perspective." Frontiers in Cellular and Infection Microbiology Volume 13 - 2023.

Macdonald, M. H., et al. (1995). "Analysis of the active site and activation mechanism of the Leishmania surface metalloproteinase GP63." Biochimica et Biophysica Acta (BBA) - Protein Structure and Molecular Enzymology 1253(2): 199-207.

Madeira, F., et al. (2022). "Search and sequence analysis tools services from EMBL-EBI in 2022." Nucleic Acids Research 50(W1): W276-W279.

McGwire, B. S., et al. (2003). "Migration through the extracellular matrix by the parasitic protozoan Leishmania is enhanced by surface metalloprotease gp63." Infect Immun 71(2): 1008-1010.

Medina, L. S., et al. (2016). "The gp63 Gene Cluster Is Highly Polymorphic in Natural Leishmania (Viannia) braziliensis Populations, but Functional Sites Are Conserved." PLOS ONE 11(9): e0163284.

Murase, L. S., et al. (2018). "The role of metalloproteases in Leishmania species infection in the New World: a systematic review." Parasitology 145(12): 1499-1509.

Olivier, M., et al. (2012). "Leishmania virulence factors: focus on the metalloprotease GP63." Microbes and Infection 14(15): 1377-1389.

Paixão, A. R., et al. (2021). Investigating the Phagocytosis of Leishmania using Confocal Microscopy, 1940-087X.

Ren, J., et al. (2009). "DOG 1.0: illustrator of protein domain structures." Cell Research 19(2): 271-273.

S, S. K., et al. (2014). "Comparative in-silico genome analysis of Leishmania (Leishmania) donovani: A step towards its species specificity." Meta Gene 2: 782-798.

Saraiva, E. M., et al. (2005). "Flow cytometric assessment of Leishmania spp metacyclic differentiation: Validation by morphological features and specific markers." Experimental Parasitology 110(1): 39-47.

Scarpini, S., et al. (2022). "Visceral Leishmaniasis: Epidemiology, Diagnosis, and Treatment Regimens in Different Geographical Areas with a Focus on Pediatrics." Microorganisms 10(10): 1887.

Schlagenhauf, E., et al. (1998). "The crystal structure of the Leishmania major surface proteinase leishmanolysin (gp63)." Structure 6(8): 1035-1046.

Shanmugasundram, A., et al. (2023). "TriTrypDB: An integrated functional genomics resource for kinetoplastida." PLoS Negl Trop Dis 17(1): e0011058.

Shio, M. T., et al. (2015). "PKC/ROS-Mediated NLRP3 Inflammasome Activation Is Attenuated by Leishmania Zinc-Metalloprotease during Infection." PLOS Neglected Tropical Diseases 9(6): e0003868.

Soteriadou, K. P., et al. (1992). "The Ser-Arg-Tyr-Asp region of the major surface glycoprotein of Leishmania mimics the Arg-Gly-Asp-Ser cell attachment region of fibronectin." Journal of Biological Chemistry 267(20): 13980-13985.

Späth, G. F., et al. (2025). "Leishmania genomic adaptation: more than just a 36-body problem." Trends in Parasitology 41(6): 441-448.

Streit, J. A., et al. (1996). "Developmental changes in the expression of Leishmania chagasi gp63 and heat shock protein in a human macrophage cell line." Infection and Immunity 64(5): 1810-1818.

Valdivia, H. O., et al. (2015). "The Leishmania metaphylome: a comprehensive survey of Leishmania protein phylogenetic relationships." BMC Genomics 16(1): 887.

van Zundert, G. C. P., et al. (2016). "The HADDOCK2.2 Web Server: User-Friendly Integrative Modeling of Biomolecular Complexes." Journal of Molecular Biology 428(4): 720-725.

Voth, B. R., et al. (1998). "Differentially expressed Leishmania major gp63 genes encode cell surface leishmanolysin with distinct signals for glycosylphosphatidylinositol attachment. Molecular and Biochemical Parasitology 93(1): 31-41.

Webb, J. R., et al. (1991). "Heterogeneity of the genes encoding the major surface glycoprotein of Leishmania donovani." Molecular and Biochemical Parasitology 48(2): 173-184.

Xue, L. C., et al. (2016). "PRODIGY: a web server for predicting the binding affinity of protein-protein complexes." Bioinformatics (Oxford, England) 32(23): 3676-3678.

Yao, C., et al. (2003). "The major surface protease (MSP or GP63) of Leishmania sp. Biosynthesis, regulation of expression, and function." Molecular and Biochemical Parasitology 132(1): 1-16.

Zackay, A., et al. (2018). "Genome wide comparison of Ethiopian Leishmania donovani strains reveals differences potentially related to parasite survival." PLOS Genetics 14(1): e1007133.